DETECTION OF POSITIVE CANCER MARGINS INTRA-OPERATIVELY DURING NEPHRECTOMY AND PROSTATECTOMY USING OPTICAL REFLECTANCE SPECTROSCOPY

by

DISHA LAXMAN PESWANI

Presented to the Faculty of the Graduate School of

The University of Texas at Arlington in Partial Fulfillment

of the Requirements

for the Degree of

MASTER OF SCIENCE IN BIOMEDICAL ENGINEERING

THE UNIVERSITY OF TEXAS AT ARLINGTON

August 2007

ACKNOWLEDGEMENTS

I would like to acknowledge all the people who helped me through out my thesis.

I take this opportunity to thank God and my parents for a constant support and inspiration at all times. It is because of their love and encouragement that I have reached here.

My sincere gratitude is expressed towards Dr. Hanli Liu for trusting my talents, for providing me constant support on this project and for building confidence in me. She has been a source of true inspiration for me.

I would also like to thank Dr. Jeffrey Caddedu who provided us with the specimens for measurements, Dr.Wareef Kabbani for helping us with the histology maps, Dr. Karim Bensalah and Dr.Altug Tuncel for providing me all the information and support that was required.

I also express my thanks to Dr. George Alexandrakis for accepting my request to be a committee member.

Finally, I thank all my lab members and friends especially Niveditha Venkatapathy and Aditya Mathker for their suggestions and cooperation from time to time during the project.

July 18, 2007

ABSTRACT

DETECTION OF POSITIVE CANCER MARGINS INTRA-OPERATIVELY DURING NEPHRECTOMY AND PROSTATECTOMY USING OPTICAL REFLECTANCE SPECTROSCOPY

Publication No. _____

Disha Laxman Peswani, M.S

The University of Texas at Arlington
and
The University of Texas Southwestern Medical Center at Dallas, 2007

Supervising Professor: Dr. Hanli Liu

In recent years optical spectroscopies have become the basis for popular research activity directed towards the development of novel, noninvasive technologies for tissue diagnostics. The motivation for my research was to eliminate the need for surgical removal of tissue samples for biopsy and histology. With the help of an optical probe placed on or near the surface of the tissue, Near Infrared (NIR) and visible light spectroscopy can provide diagnostic signatures, non-invasively and in real time. While the ultimate goal of my research development is the elimination of the need to remove t

issue samples, the technology that I am developing can also be used to provide additional guidance in real time during laparoscopic surgery.

In this study, optical reflectance spectroscopy with short source-detector separation is used as a minimally invasive technique to differentiate normal tissues from tumor lesions ex-vivo. Reflectance spectra (400 nm – 1000 nm) were acquired with an optical probe from human specimens after radical or partial nephrectomys and radical prostatectomy. The main aim of my thesis was to differentiate between normal and tumor tissues and then extend the application to differentiate between benign and malignant tissues. The study involved 13 human subjects' specimens for prostate measurements and 23 human subjects's specimens for kidney measurements. My study reveals that for kidney tissues, promising parameters were (1) the slope of the reflectance spectrum from 630 nm to 900 nm, (2) correlation coefficients between the normal and tumor (or between benign and malignant) reflectance spectra from 560 nm to 630 nm, (3) and two-wavelength-intensity classifications. For prostate tissue, promising parameters were the slope of the reflectance spectrum from 630 nm to 900 nm. Furthermore, NIR reflectance spectroscopy can be further used with an optical probe having larger source-detector separations to image deep tissues. A "smart" probe can be designed which can be used intra-operatively to provide real time surgical guidance during laparoscopic surgery.

TABLE OF CONTENTS

LIST OF ILLUSTRATIONS

LIST OF TABLES

CHAPTER 1

INTRODUCTION

1.1 Anatomy and Physiology of Kidney

The Kidneys are bean shaped exocrine glands found in the posterior part of the abdomen, one on each side of the spine as shown in Figure 1.1.

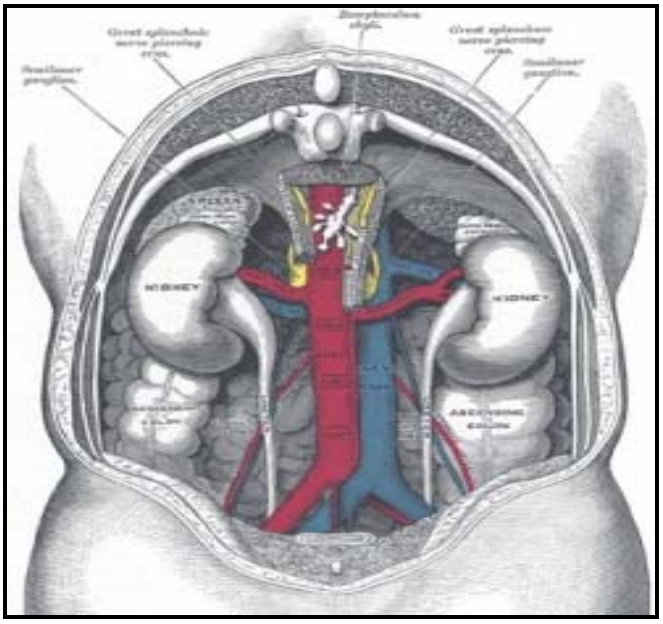

Figure 1.1 Anatomical locations of the kidney and the other organs [1]

The kidneys can be divided into two parts based on their functions. The outer region is called the Cortex, and it is responsible for filtration of blood. The inner region is called the Medulla which is responsible for the filtration of urine. The inner region is

also called the renal pelvis. The kidney has a thin, non-elastic collagen capsule, which participates in auto regulation of renal blood flow. Figure 1.2 gives an inner view of the kidney.

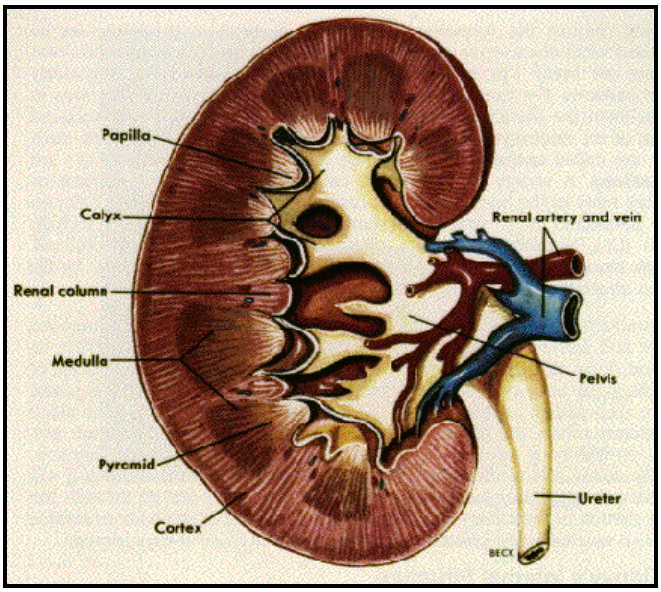

Figure 1.2 Internal structure of the kidney

The basic functional unit of the kidney is the nephron, of which there are more than a million within the cortex and medulla of each normal adult human kidney. Each nephron contains the glomeruli and a tubule. The main functions of the kidney are to filter waste materials from the blood and excrete these wastes in the form of urine; they also regulate the amounts of water and other chemicals in body fluids. The waste products filtered from the blood are collected in the renal pelvis of the kidney. These then pass through the ureter and out as urine. Kidney is also important in the release of vital hormones into the bloodstream such as renin and erythropoietin.

Kidney cancer is one of the most cancers affecting male and is diagnosed between the ages 50 and 70 years. The most common kidney cancer is the renal cell carcinoma, which accounts for 85% of the kidney tumors. [1]

1.1.1 Radical Nephrectomy

This is the process for the removal of the kidney tumor. In this surgery, the physician will remove the whole kidney and the surrounding tissues including the adrenal gland. Some of the lymph nodes are also removed in the surgery. In the surgery, an incision is made in front or side of the abdomen. Sometimes in the case of large tumors, the incision may extend up to the chest. By this surgery the kidney and its affected parts are removed.

1.1.2 Partial Nephrectomy

In this procedure the some of the kidney is left behind in the surgery and hence the name Partial. The parts infected with cancer and surrounding fat tissue is only removed. This is done generally in the early stages of cancer. This surgery is also called the nephron sparing surgery as a part of the kidney is still working. This is usually done for people with stage 1 cancer [2].

1.2 Anatomy and Physiology of Prostate Gland

The prostate gland is an exocrine gland which is the size of a walnut, it is found just at the base of the urinary bladder, and it surrounds the urethra (see Figure 1.3). The prostate gland is a part of the male reproductive system.

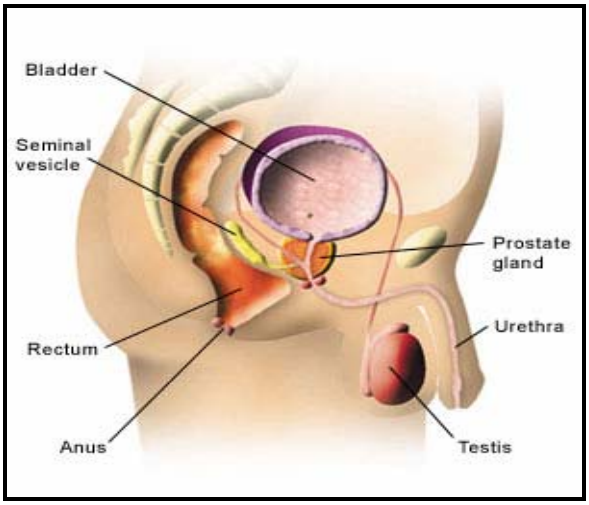

Figure 1.3 Location of the prostate

The function of the prostate gland is to control urination, and this is done when it presses against the surrounding urethra. Behind the prostate are the seminal vesicles in the form of two small sacs that store the sperm cells. These seminal vesicles pass through the prostate gland and connect to the urethra. Another function of the prostate is to secrete the seminal fluid. The prostate also contains smooth muscles that help in expelling the semen during ejaculation [3]. Figure 1.4 provides some graphical information on the prostate anatomy.

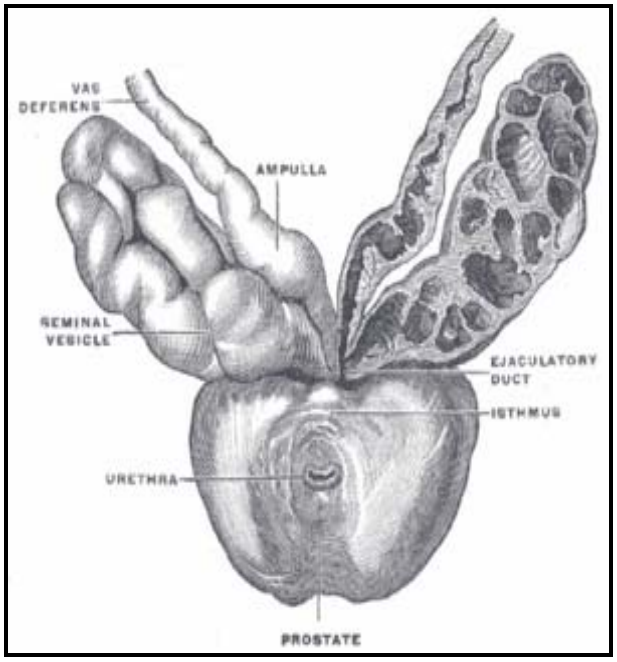

Figure 1.4 Prostate gland with the seminal vesicles

The prostate gland is divided based on zones for pathological reasons. The zones of the prostate are as follows:

- **The Peripheral Zone** –It comprises of the 70% of normal prostate gland in young men. This is the major origination of prostate cancers.
- **The Central Zone** –It comprises of 25% of prostate gland and also 25% origination of prostate cancer.
- **The Transition Zone** –It is comprised of 5% of prostate volume and is rarely associated with carcinoma.
- **The Anterior Fibro muscular Zone –** It is composed of muscle and fibrous tissue and adds to 5% of prostatic weight [4].

1.2.1 Growth of a prostate

The prostate gland is very small at the time of birth. The growth of the prostate occurs during puberty which is induced by the testosterone which is the male sex hormone. The prostate continues to grow due to the enlargements of glands and due to the muscle present within the prostate. This enlargement of the prostate gland with age is called Benign Prostatic Hypertrophy (BPH). However the BPH is not associated with cancer. The prostate cancer occurs in nearly 60% of the male population and is generally found in older men.

1.2.2 Prostate Cancer

For prostate cancer suspects, doctors follow up an elevated PSA (Prostate Specific Antigen) or positive DRE (Digital Rectal Examination) with more definitive testing. Some physicians employ Trans-rectal ultrasound (TRUS), which uses a rectal probe that creates a video image of the prostate using harmless sound waves collected by a computer. TRUS helps the physician decide if a biopsy is needed. If so, the doctor will take tiny prostate tissue samples with a small-gauge needle, injected typically through the rectum. Another physician, a pathologist, then examines the samples under a microscope after the prostate samples are collected. Once cancer is diagnosed, other tests such as computerized tomography, lymph-node biopsies, and bone scans can be used to determine if tumors have spread beyond the prostate.

With the prostate cancer, treatment means either removing the gland (i.e., radical prostatectomy) or bombarding it with radiation. Experts say that these options may offer good prospects for curing the disease if exercised early enough. Surgery may

cause unpleasant adverse effects. Because radical prostatectomy can result in severing nerves and blood vessels related to sexual or bladder function, the operation in the past has left virtually all patients impotent, incontinent, or both.

Not all prostate cancer is equal. One type of tumor may lie dormant for years while another is virulent and deadly. Also important is "staging"--a predictor of how extensively the disease has grown within or beyond the prostate [5].

1.2.3 Laparoscopic Prostatectomy

This is a process by which prostate and seminal vesicles are removed in order to prevent cancer. This technique is a minimally invasive technique i.e. there is a less amount of blood loss, less pain and fast recovery. Small incisions are done on the abdomen that allow the instruments and the video camera to pass through. The video camera helps the physician to monitor the surgery.

1.2.4 Radical Prostatectomy

This is a surgery performed with a general anesthesia in order to remove the entire prostate gland. In this process an incision is made below the navel and extends until just above the pubic bone. During the surgery a catheter is passed through the urethra into the bladder. This catheter is later then removed after a few weeks. The process helps in the prevention of cancer from further spreading to other parts of the body [6].

1.3 Background of Optical Spectroscopy

The optical spectroscopy I used in my study consists of two parts: Near infrared spectroscopy (NIRS) and visible spectroscopy. NIRS is a spectroscopic method utilizing the near infrared region (from about 800 nm to 2500 nm)[7], and the visible

spectroscopy uses light from 400 nm to 700 nm of the electromagnetic spectrum. The primary application of optical spectroscopy (both NIRS and visible light spectroscopy) to the human body uses the fact that the transmission and absorption of light in human body tissues contain information about hemoglobin concentrations.

The depth of penetration of visible light (400 nm- 700 nm) is much shorter than that of the NIR wavelength (700 nm-1100 nm). Thus, the visible light detects signals from the more superficial layers than the NIR. This is of particular importance when the sample to be analyzed is heterogeneous.

Traditional NIR analysis has used diffuse reflectance sampling. This mode of sampling is convenient for samples/specimens that are highly light scattering or samples for which there is no physical means to employ transmission spectroscopy. Diffusely reflected light is light that has entered a sample, undergone multiple scattering events, and emerged from the surface in random directions. Besides scattering, a portion of light that enters the biological sample is also absorbed, which is highly noticed in the visible region, mainly by the presence of blood or hemoglobin. The depth of light penetration is highly dependent on the sample characteristics and is often affected by the size of scattering particles in the sample and the sample density [8].

If the sensing optical probe has a small source-detector separation, either for NIR or visible light, there is no good theory to follow. Thus, visible to NIR spectral analysis is largely an empirical method; tissue spectroscopy using small-separation probes is frequently carried out using emphirical approaches and/or with calibration procedures.

1.3.1 Behavior of light inside the tissue

When light enters a tissue, its propagation is mainly governed by two physical phenomena, i.e., light absorption and scattering. There are certain substances in human tissues for which optical spectra within both visible and NIR wavelengths are well defined. Some of these absorbers such as water, melanin, and bilirubin do not change in concentration with time. But concentrations of some other absorbers such as oxygenated hemoglobin (HbO2) and deoxy hemoglobin (Hb) are strongly related to the tissue oxygenation and metabolism. Thus the absorption changes can provide clinically useful physiological information [9]. Figure 1.6 shows absorption spectra of water, and Figure 1.7 shows absorption spectra of Hb and HbO2. As can be seen from these spectra, water absorption dominates at wavelengths above 1000 nm, whereas below 650 nm there is a dominant absorption by both Hb and HbO2. Thus a so called 'near infrared window' is defined in the range from 650 nm to 1000 nm, which is considered useful for the non-invasive NIR measurements.

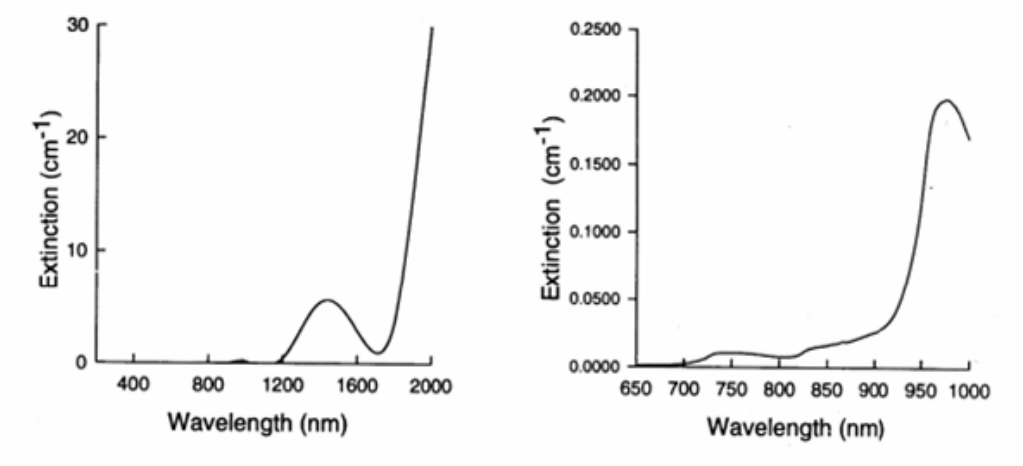

Figure 1.6 Absorption Spectra of pure Water [8]

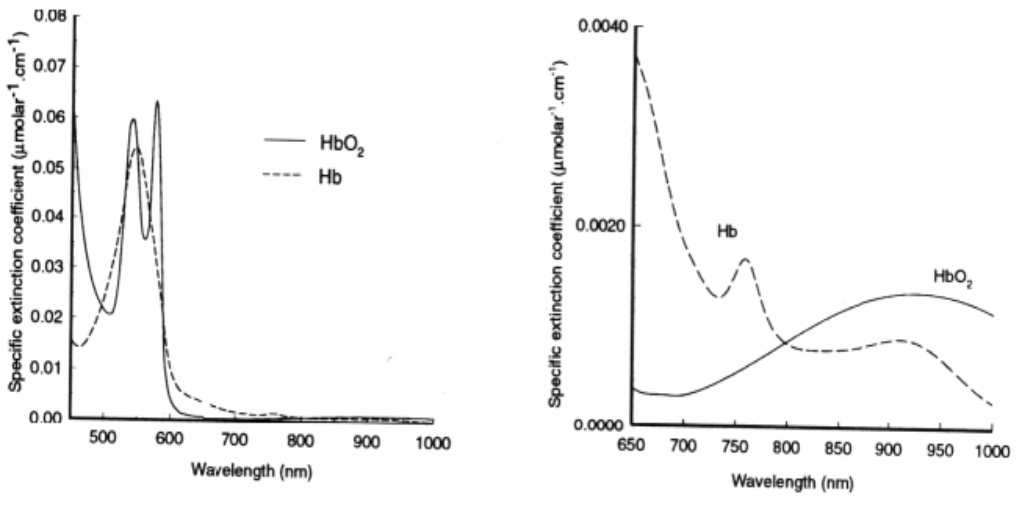

Figure 1.7 Absorption Spectra for Hb and HbO_2 [8]

1.4 Research Outline

The focus of my project was to develop a technique which could differentiate tumor tissues from normal tissues in both kidney samples and prostate samples.

The first part of this thesis highlights the experimental protocol, instrumentation and the results obtained from 23 human kidney samples. After successfully completing the analysis on these 23 kidney samples and observing that this technique could help differentiate tumors from normal tissues, the application was further extended trying to detect positive margins in case of partial kidney samples. The results were found to support the feasibility to use optical spectroscopy (both visible and NIR) for guiding surgical tumor removal with an adequate normal parenchyma margin. Moreover, I next explored and proved the feasibility to differentiate benign and malignant kidney tumors using the similar approach. Since benign tumor cells grow only locally and do not spread by invasion or metastasis, they are considered to be harmless to health. Hence, if

this technique can differentiate benign from malignant tumors, the unwanted surgery can be avoided.

The second part of my project uses the same technique, but for another surgical-related application. The next part of the body on target is the prostate gland. For prostate early diagnosis and treatment, one urgent need is to have an instrument which would enter through the rectum, would be minimally invasive, and could detect prostate tumors at an early stage so that they could be treated without surgery.

Also, during prostatectomy, one of the major issues is to separate the prostate from the critical surrounding tissues and to use the harmonic scalpel to develop a plane between the gland and the Neurovascular bundle (NVB). A harmonic scalpel is the tool that uses ultrasound technology to seal tissues while it is cutting. Anatomic studies have demonstrated the precise location of the neurovascular bundle, with which most urologists are familiar. But still, the continuous venous bleeding narrows pelvic surgical field and leads to poor visibility which adversely impacts nerve preservation (as shown Figure 1.8). Hence, we can think about using the same optical tool to guide laparoscopic surgery for nerve sparing, i.e. basically to guide the surgeons during laparoscopic prostatectomy.

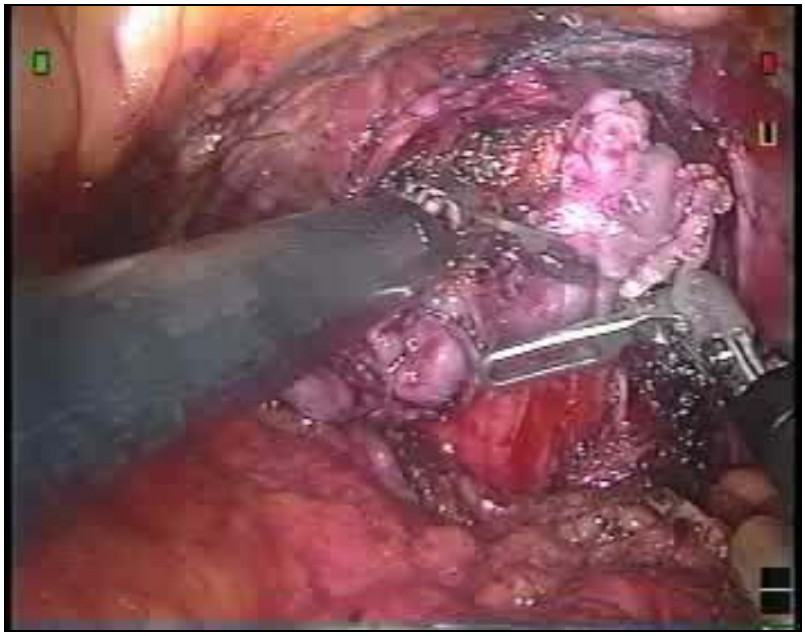

Figure 1.8 Laparoscopic Prostatectomy

To fulfill this motivation, our research team conducted the testing phase by making ex vivo measurements on 13 human prostate samples. I have analyzed the data from 5 of them and found them to be satisfactory. This suggests that more human specimen measurements need to be carried out to prove that optical (visible and NIR) spectroscopy can differentiate prostate tumor tissues from normal tissues and thus to be useful for guiding laparoscopic prostatectomy in vivo in real time.

CHAPTER 2

INSTRUMENTATION

The experimental set-up (Figure 2.1) for optical spectroscopic measurements consisted of a spectrometer (USB 2000, Ocean Optics, Inc., Dunedin, FL) having a wavelength range from 400 nm to 1000 nm (covering both visible and NIR spectra), a tungsten-halogen light source (HL-2000, Ocean Optics, Inc., Dunedin, FL), a laptop computer which had a Lab View interface software (National Instruments, Austin, TX) for collecting and displaying the optical reflectance curves in real time, and a fiber optic array probe which consisted of 7 splitters (See Figure 2.2). The distance between two neighboring splitters was 100 μm. For kidney measurements, the splitter #3 was connected to the light source and the splitter #5 connected to the spectrometer. Hence we used a fiber optic probe having a 200 μm separation between the source and detector. The reflected signal passed through the optical fiber was detected by the spectrometer and the signal of the spectrometer output sent to the computer.

The experimental setup for the prostate measurements was similar to the system mentioned above except that it was measured by a bi-furcated fiber optic probe (Figure 2.3(b)), instead of the fiber array probe, and that the light source used was a tungsten-halogen light source (LS-1, Ocean Optics, Inc., Dunedin, FL) (Figure 2.3(a)). The Ocean Optics interface software was used on the computer to display the optical reflectance curves. Figure 2.4 shows the environment and the setup used for both the

kidney and prostate specimen measurements, which were taken place in a pathology laboratory very close to the operating room.

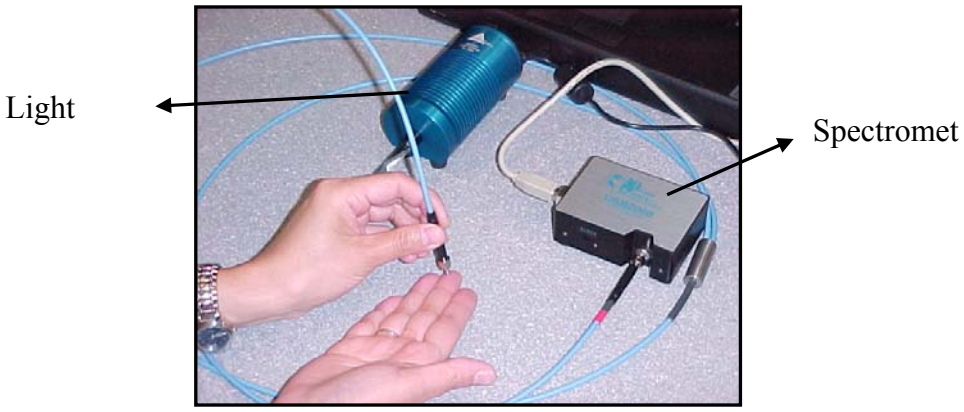

Figure 2.1 Experimental setup for the reflectance measurements of kidney sample

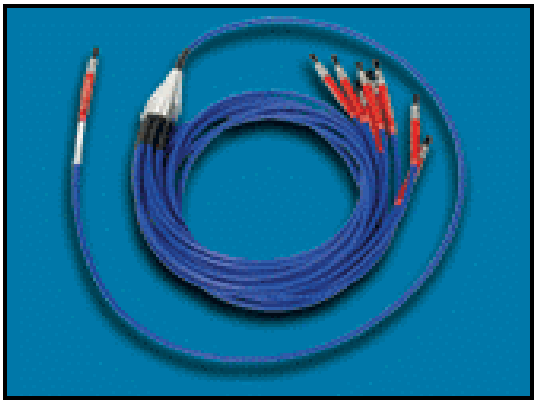

Figure 2.2 A fiber optic array probe [10]

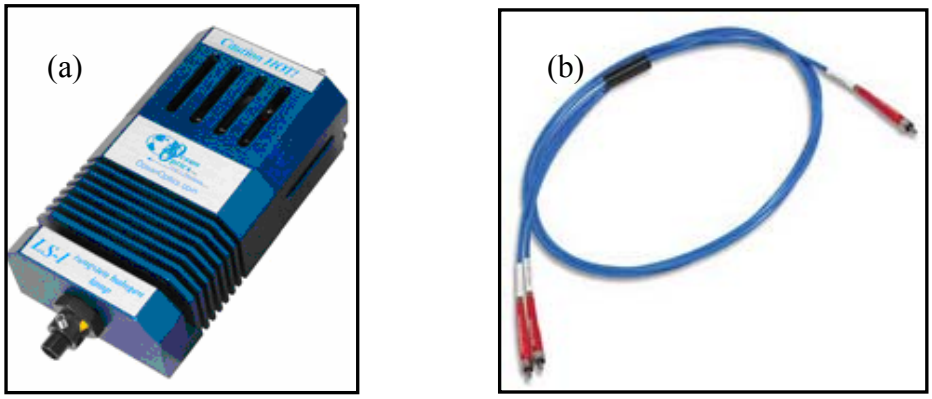

Figure 2.3 (a) LS-1 tungsten halogen light source and
(b) a bi-furcated fiber optic probe.

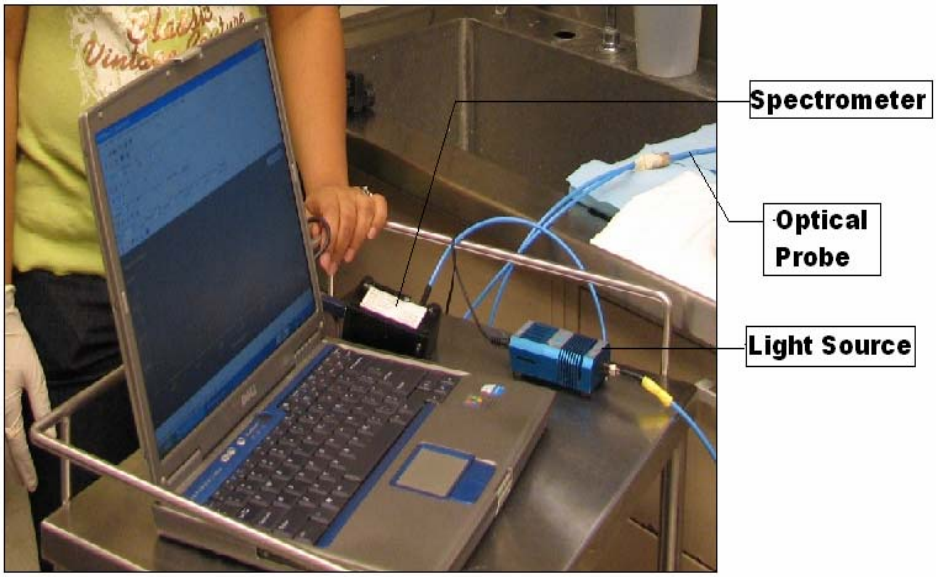

Figure 2.4 Experimental setup for the reflectance measurements
of prostate sample

The fiber optic probe used for the prostate sample measurements contained two 400-µm diameter fibers for light delivery and light collection, respectively, with an outer diameter of 1.3 mm. The center-to-center distance between the source and detector fibers was approximately 400 µm. A cross-section drawing for the 400-µm probe is shown in Figure 2.5.

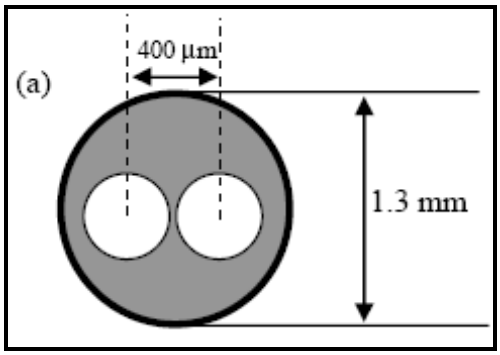

Figure 2.5 The schematic cross section of the 400-µm fiber probe [11]

The effects from the fiber, light source and spectrometer were removed by dividing each optical reflectance signal by a calibration curve which was taken from a 100% reflective surface. The sample provided ~100% reflectance in the wavelength range of 250 nm to 2500 nm (Diffuse Reflectance Standard Specifications, Ocean Optics, FL).

CHAPTER 3

SPECTROSCOPIC MEASUREMENTS ON THE KIDNEY SAMPLE EX-VIVO

Data was collected from the patients' removed kidney specimens, and the patients had undergone laparoscopic nephrectomy at University of Texas Southwestern Medical Centre at Dallas. The study was approved by the Institutional Review Board of The University of Texas at Arlington and University of Texas Southwestern Medical Centre at Dallas (UTSW).

Spectroscopic measurements were made on the kidney samples of 23 patients using the optical (visible + NIRS) system. Of these 23 patients, 9 patients had undergone partial nephrectomy and 14 patients undergone radical nephrectomy. Amongst these numbers of cases, two cases were excluded after the histology results were obtained. One case was a Transitional Cell Carcinoma and the other was a Hemorrhage cyst.

3.1 Need for in vivo surgical guidance

During laparoscopic partial nephrectomy, when the surgeon tries to remove the tumor, a real-time guidance tool is needed which would be minimally invasive and tell him/her instantly if the tissue the guiding tool touches is a normal parenchyma or a tumor tissue. In other words, when referring to the optical spectroscopic measurement map, as shown in Figure 3.5, the instrument would tell the surgeon whether the

measured tissue (characterized by curve #5) is similar to normal tissues (given by curve #4 and #6) or it is similar to the tumor tissues (given by curve #7 and #8).

For similar purposes, intraoperative frozen section analysis of the specimen is usually performed during open surgery or even for laparoscopic surgery. To complete the frozen section analysis, it usually takes about 15-20 minutes. The surgery has to wait with the possibility that the positive tumor/cancer margins exist; thus, the frozen section analysis becomes very time consuming, non-efficient, and un-safe to the patients. This issue exists for both laparoscopic nephrectomy and laparoscopic prostatectomy

Hence, the basic requirement or development for my study was to have a portable instrument which would be minimally invasive and provide real-time, fast optical signatures which would differentiate normal and tumor efficiently. Furthermore, before the surgery, although laboratory tests or/and other imaging examinations have been performed, the surgeon and the patient are not sure about the tumor type. Therefore, it is also important to have an instrument which could differentiate benign from malignant tumors in kidney.

3.2 Sample Preparation and Experimental Protocol

After the sample was removed from the patient's body, it was put on ice in a bucket and taken to the pathology department of UTSW. The tumor size was measured first, followed by the optical measurements. For the optical measurements, there was a kidney chart prepared separately for radical (Figure 3.2) and partial nephrectomy (Figure 3.5). The experimental set up for the optical measurements was mentioned in

Chapter 2 (Figures 2.3-2.4). The kidney charts allowed the measurements to be repeated at the relatively similar position/location consistently on every sample. The actual measurements from the kidney specimens were taken by Drs. Karim Bensalah and Altug Tuncel, who were practicing urologists and visiting scholars with Dr. Cadeddu at UTSW at the time of measurements.

Dark background was recorded at the start of each measurement, keeping the same settings, but having the tungsten-halogen light source switched off. Later during data analysis, this background data was subtracted from each reflectance measurement. Similarly at the end of each measurement, reflectance readings were taken from the Ocean Optics white sample, keeping the settings same as those during the measurements on the kidney sample. The white sample serves as a 100% reflective surface for spectral calibration. During data processing, after subtracting the background from each reflectance measurement, it was divided by the white sample reflectance reading. This was basically done to cancel the spectral effects due to the spectrometer, light source or the optical fiber during sample measurements.

Figure 3.1 An example of the entire kidney removed from a patient and obtained after laparoscopic radical nephrectomy.

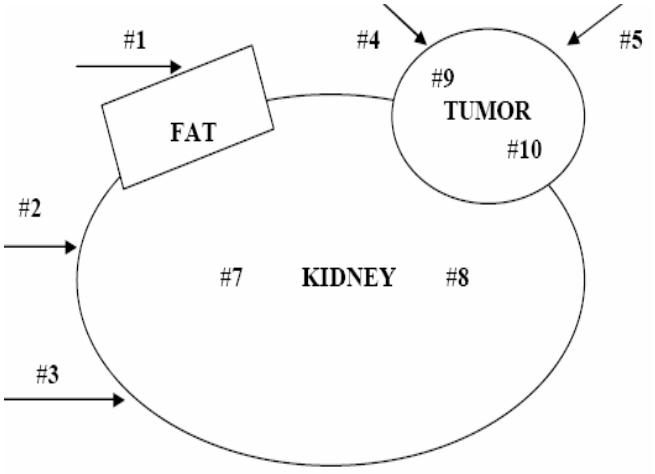

Figure 3.2 A location map to identify the positions for the optical spectroscopic measurements from a radical kidney

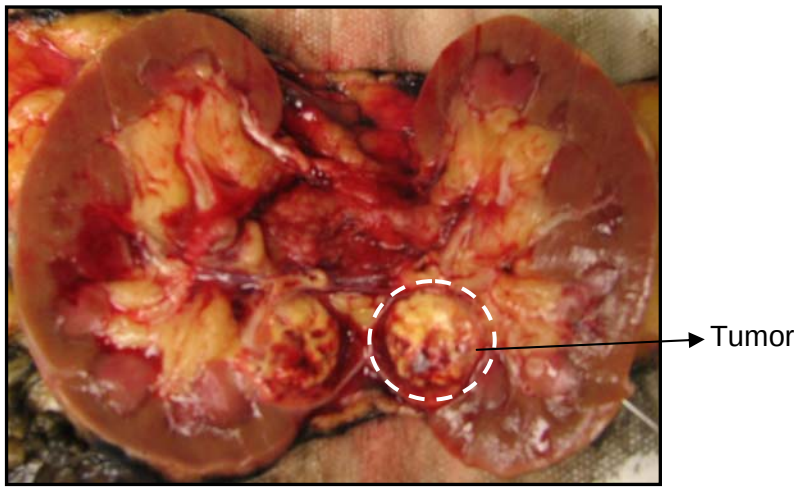

Figure 3.3 A whole kidney after cutting it into two halves

Now, for a radical kidney sample (Figure 3.1), as shown in Figure 3.2, the reflectance measurement on position #1 was taken on the perirenal fat, #2 and #3 readings were on the capsule with no traces of tumor, #4 and #5 readings were the measurements on the surface of the tumor, #6 was on the fat surrounding the tumor, #7 and #8 were the readings taken on normal parenchyma after bi-halving the kidney

sample, as shown in Figure 3.3, and #9 and #10 were the readings taken on tumor surface after bi-halving the kidney sample. This experimental protocol was followed for every radical kidney sample.

For partial kidney samples (Figure 3.4), the same reflectance measurements were taken at the start and end of the experiment protocol, and similar data processing analysis were followed as those used for the radical kidneys. The optical spectroscopic measurement chart for partial kidney (Figure 3.5) was different than that for radical kidney (Figure 3.2).

As shown in Figure 3.5, the reflectance measurement on position #1 was taken on the peritumoral fat, #2 and #3 were the measurements on the surface of the tumor, #4 and #6 was on the parenchyma which was adjacent to the tumor, #5 was the thinnest parenchyma section adjacent to the tumor after bi-halving the kidney sample, and #7 and #8 were the readings taken on tumor surface after bi-halving the kidney sample (Figure 3.6). This experimental protocol was followed for every partial kidney sample.

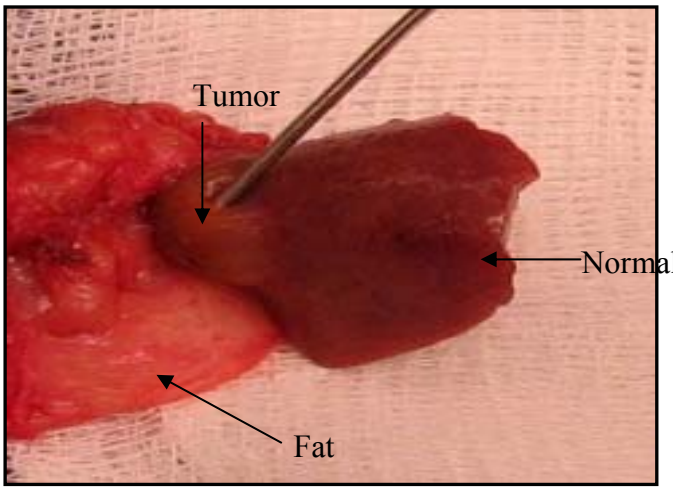

Figure 3.4 Example of a partial kidney removed from the patient after laparoscopic partial nephrectomy.

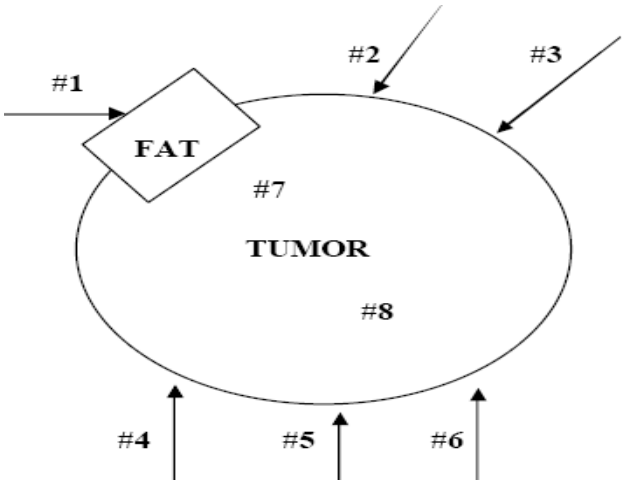

Figure 3.5 An optical spectroscopic measurement map for partial kidney

Figure 3.6 The partial kidney shown in figure 3.4, after cutting it into two halves

3.3 Data analysis using the technique of difference in slopes

As mentioned in Section 3.1, spectroscopic measurements were done on 21 kidney samples, of which 8 measurements were on partial kidneys and 13 measurements were on the whole kidneys, i.e. radical kidneys. After subtracting by the dark background reflectance measurements and then dividing them by the white sample,

the data were normalized in such a way that the reflectance intensities between 450 nm and 850 nm on Y axis would fall between 0 and 1 for each spectrum.

The above mentioned data analysis technique was done only on the sample after it was cut into two halves. After bi-halving, there were 48 sites measured on normal parenchyma (from both radical and partial) and 40 sites on tumor (also from both radical and partial). The mean of 48 curves provided with one normal curve, and similarly the mean of 40 curves gave one tumor curve, as shown in Figure 3.7.

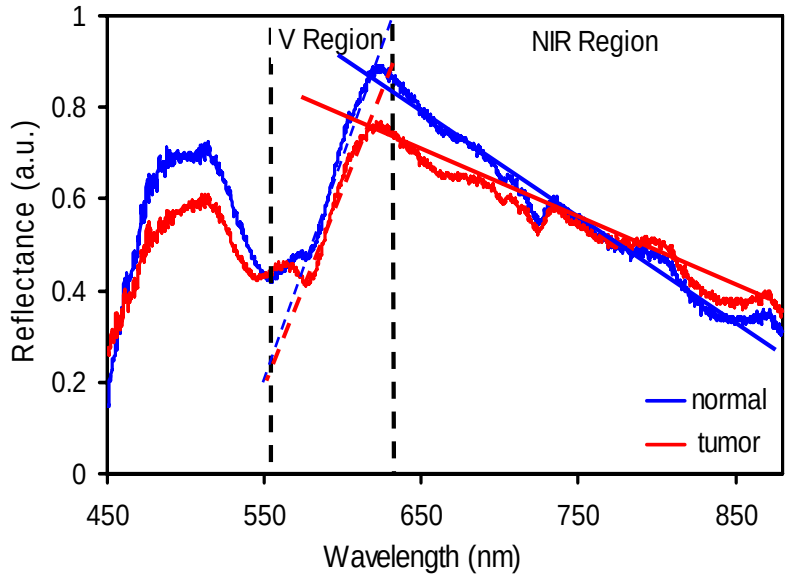

Figure 3.7 The average normal curve (mean from 48 normal sites) and average tumor curve (mean from 40 tumor sites)

As shown in Figure 3.7, the curves were divided into two regions, the NIR region and the visible region, for data analysis. The NIR region was from 630 nm to 880 nm, and the visible region was from 570 nm to 630 nm. The spectral slopes were calculated for the mean reflectance curves in the NIR region (red and blue solid lines) and the visible region (red and blue dashed lines). A student t-test was used to check the

differences between the normal and tumor tissues. A student t-test is a fundamental statistical process to compare the two means of two groups of data. Normally, if p is less than 0.05 ($p<0.05$), the two means of the two groups are significantly different; if $p>0.05$, the two means have no differences.

3.4 Data analysis using the correlation calculation method

The correlation calculations were done in the visible region of the spectrum which ranges from 560 nm to 630 nm.

The correlation coefficient basically reflects the extent of a linear relationship between two data sets. The closer the coefficient is to 1, the stronger the correlation is between the variables. In this broad sense there are several coefficients, measuring the degree of correlation, adapted to the nature of data.

The kidney data analysis was done using the Pearson method. The formula for Pearson's calculation [12] is defined as follows:

$$r = \frac{\sum XY - \frac{\sum X \sum Y}{N}}{\sqrt{(\sum X^2 - \frac{(\sum X)^2}{N})(\sum Y^2 - \frac{(\sum Y)^2}{N})}} \qquad (1)$$

where r is the Pearson's correlation coefficient, and x and y are two variables that need to be tested for their linear relationship. For our data analysis using Pearson's correlation calculation, the spectral data sets were not normalized: After subtracting the dark background, the spectral data were divided by the white sample. While the calculation of correlation does not require non-normalized data, I would like to check whether non-normalized data could yield some useful results.

The correlation calculations were not performed in the NIR region since the correlation coefficients would be near 1 all the time between the spectra of tumor and normal tissue in the NIR region. The basic principle behind this statement results from the linear spectral feature between 630 nm to 880 nm obtained for both tumor and normal tissues (Figure 3.7). Mathematically, we can prove it as follows:

y_1 is the tumor spectrum (630-880 nm) and is equal to: $y_1 = k_1\lambda + b_1$,

y_2 is the normal tissue spectrum (630-880 nm) and is equal to: $y_2 = k_2\lambda + b_2$;

If combining the two equations and canceling λ, we will get

$$y_1 = (k_1 / k_2)* y_2 + [b_1 - (k_1 / k_2)* b_2]. \qquad (2)$$

Equation (2) is a perfect linear equation, with a slope of k_1/k_2 and an intercept of $[b_2 - (k_1 / k_2)* b_2]$. It indicates mathematically that the two linear lines, y_1 and y_2, will be correlated nearly perfectly if y_1 and y_2 are good linear lines, regardless of the individual values of k_1 and k_2. Hence, I do not calculate correlation coefficients in the NIR region.

3.5 Results

3.5.1 Results obtained from the slope calculation method

As mentioned earlier, there were 48 sites measured from normal parenchyma and 40 sites from the tumors, combining both the partial and radical nephrectomies. The optical spectra for the normal and tumor tissues were shown in Figure 3.7. The spectra displayed the mean of the 48 spectra for normal and the mean of 40 spectra for tumors.

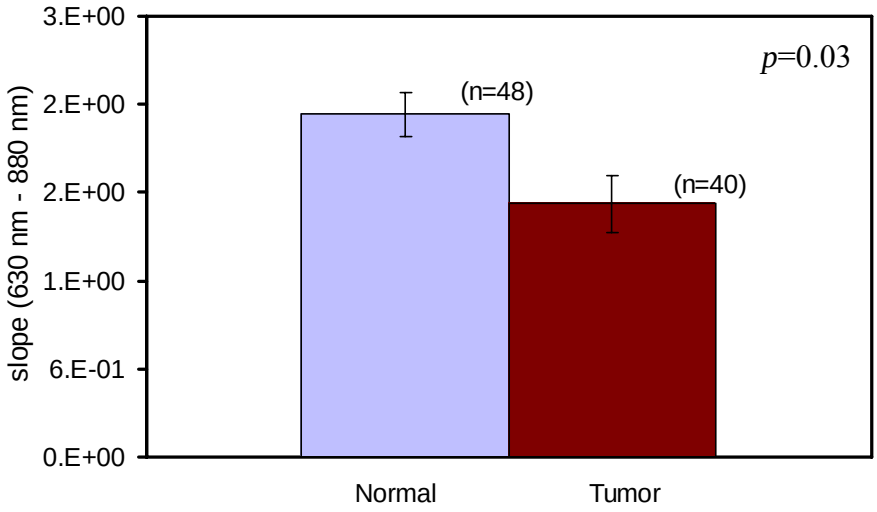

Figure 3.8 Difference in slopes in the wavelength range from 630 nm to 880 nm, obtained with the NIRS measurements from kidney samples

In the NIR region and the visible region, the slopes of all qualified individual spectra were calculated, and the representation of the slopes is displayed on a bar graph in Figure 3.8. A student t-test was performed to find the differences between the two groups. The p-value for the NIR region was found to be 0.03 which is less than 0.05. Hence there was a significant difference in the NIR spectral slopes between the normal parenchyma and tumor tissues.

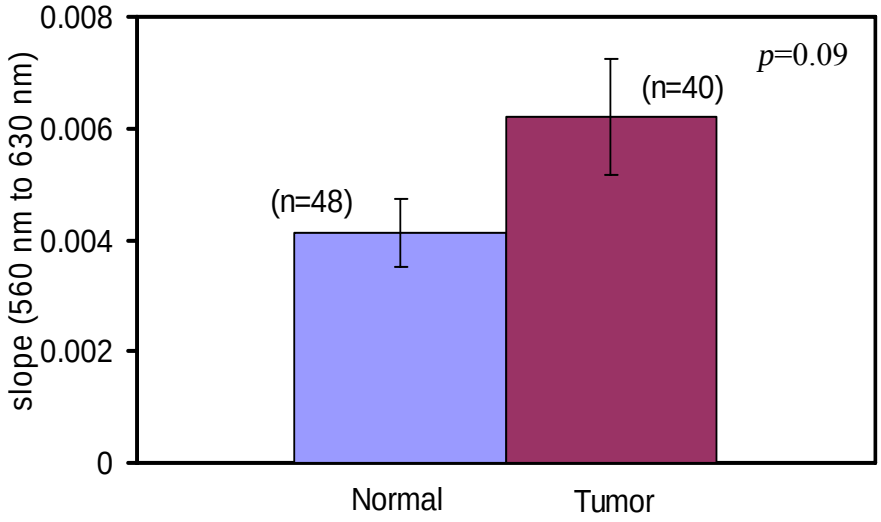

Figure 3.9 Difference in slopes in the wavelength range from 560 nm to 630 nm, obtained with the optical spectral measurements from kidney samples

Similar to Figure 3.8, Figure 3.9 displays the difference in slopes between the normal tissues and tumor tissues in the visible region, calculated from 560 nm to 630 nm. The p-value was found to be 0.09, indicating that there is no significant difference between the normal tissues and tumor tissues in the wavelength range of 560 nm to 630 nm. The reason for this is that considering all the kidney samples, 50% of them were oncocytoma histology subtype, and the rest 50% were clear cell histology subtypes. Among these clear cell histology subtypes, all of them (i.e. 100%) had higher reflectance intensities for tumor tissues and in the oncocytoma histology subtypes, 75% of them had lower intensities for tumor tissues which I think is the property of these histology subtypes. So I tried separating the oncocytoma subtype data from the clear cell subtype. I excluded the data from the oncocytoma subtype data in both normal and tumor cases. After comparing the slopes of clear cell histology subtypes, I obtained the

results as shown in Figure 3.10. The p-value obtained through the statistical student t-test was found to be 0.03. Hence we see a significant difference between the normal tissues and tumor tissues after separating the oncocytoma subtypes from the clear cell subtypes in the wavelength range of 560 nm to 630 nm.

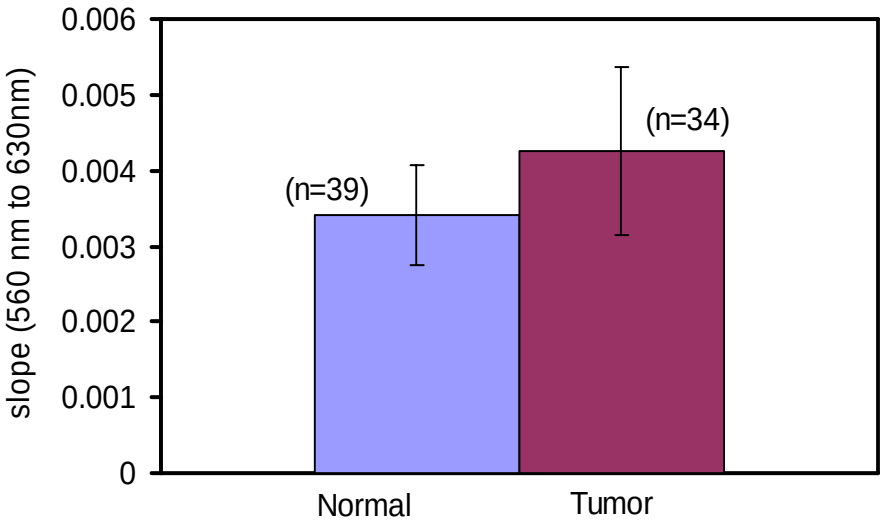

Figure 3.10 Difference in slopes in the wavelength range from 560 nm to 630 nm, after separating oncocytoma histology subtypes from clear cell histology subtypes.

3.5.2 Results obtained from the correlation calculation method

To detect the positive margin, apart from calculating the slopes, the correlation coefficients were calculated in the visible region, as an additional possible method to differentiate the tumor tissues from normal tissues.

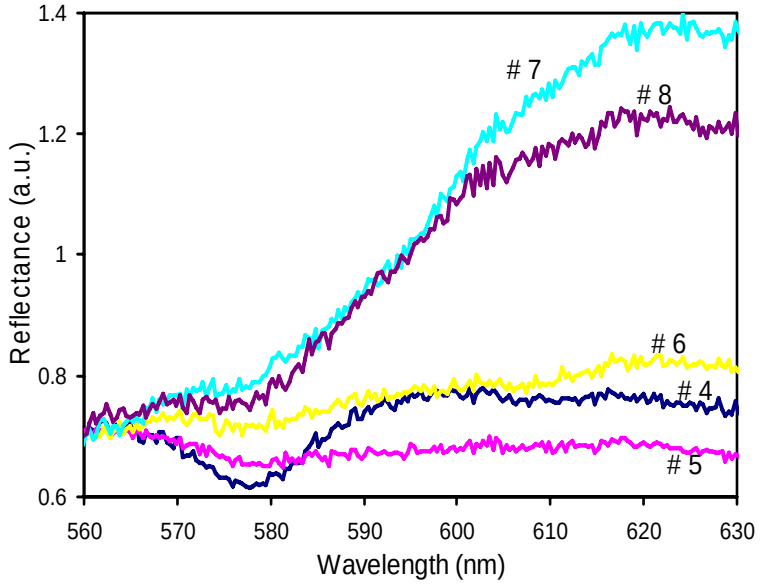

Figure 3.11 Optical reflectance curves from a kidney sample after subtracting the background and dividing by white sample spectrum

Figure 3.11 show the optical signatures obtained after subtracting dark background and dividing by the white sample spectrum. The set of reflectance data was from a patient who had undergone a partial nephrectomy surgery on the 22nd January 2007. The histology results showed that it was an oncocytoma case. After the frozen section analysis of this case, it was found that the surgeon had cut safe through the tumor, which means that there was no positive margin seen.

In Figure 3.11, the curve #4 and #6 are from normal parenchyma and #5 is from the thinnest parenchyma which is adjacent to the tumor. The curve #7 and #8 are from the tumor sections. Since curve #5 lays along with #4 and #6 and it is well separated from curve #7 and #8, we can prove, using our optical spectral readings, the fact that there is no positive margin,. A quantitative way to prove this point is to obtain correlation coefficients among those curves/spectra in the visible region (560-630 nm).

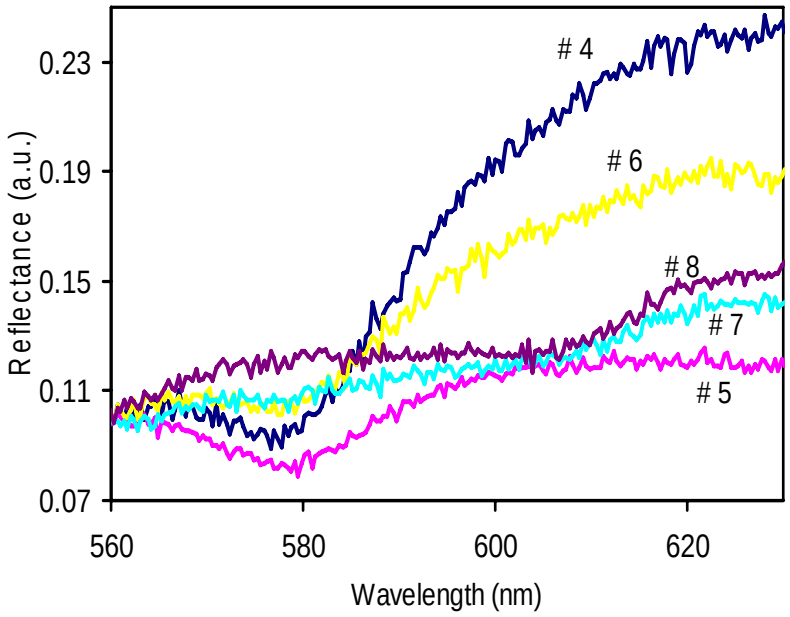

Figure 3.12 Optical reflectance curves from another kidney sample after subtracting background and dividing by white sample spectrum.

Figure 3.12 plots the visible spectra from 560-630 nm from another kidney specimen, again obtained from non-normalized data. The reflectance data are taken from a patient who had undergone a partial nephrectomy surgery, and the histology results showed that it was an oncocytoma case. Further frozen section analysis suggested that there was a positive margin during this surgery, which means while cutting through the tumor, there was tumor tissues left with the patient.

As seen from the above figure, curve #5 lies along with curves #7 and #8 which were taken from tumors. Curve #4 and #6 are still well separated from the tumor curves (#7 and #8). This figure means that the optical spectral signature can indicate a positive margin consistently with the histology data. Quantitatively, calculation of correlation

coefficients may be also able to identify the positive margin by displaying the numerical values of correlation.

Table 3.1 Correlation coefficient values between two tumor positions (#7 and #8 in partial optical spectroscopic map) along with their slopes in the wavelength range from 630 nm to 880 nm.

	C/C		
	slope of curve 7	correlation between pts(7,8)	slope of curve 8
	2.26	0.99	2.49
	2.09	0.97	2.22
	1.85	0.94	2.04
	1.25	1.00	1.88
	2.03	0.98	1.97
	1.92	0.99	2.15
Mean	1.90	0.94	2.12
Stdev	0.32	0.16	0.35
SEM	0.13	0.06	0.14

Table 3.1 represents the correlation coefficients between the two tumor positions (as labeled C/C). Each row in the table represents one case. Thus, the mean calculated in the table is from 6 cases. Namely, the correlation coefficient between curve #7 and curve #8 is calculated in the wavelength range from 560 nm to 630 nm and listed in the middle column in the table. The slopes of curves #7 and #8 from 630 nm to 880 nm are also given in the first and third columns, respectively (The slope values in the table have been multiplied by a factor of 1000).

As seen from the table, the middle column,i.e., the correlation values between the two tumor positions, are near to 1, indicating a good correlation between the two. Consistantly, the mean slope of multiple curve #7 (-0.0019) is very consistent with that of curve #8 (-0.0021). Furthermore, Figure 3.13 presents a graphical representation for correlation between curve #7 and curve #8, showing a correlation of 0.99.

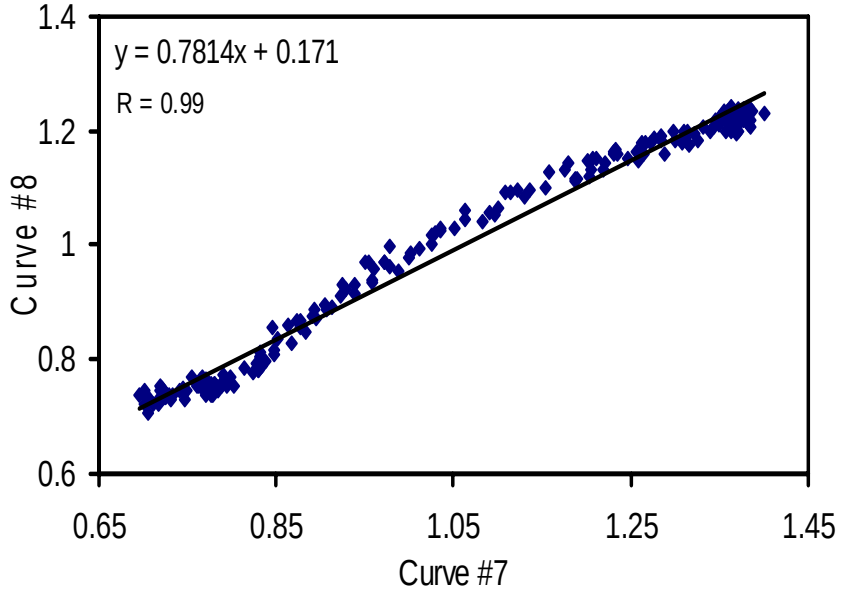

Figure 3.13 A graphical representation of the correlation calculation method between curve #7 and curve #8.

Table 3.2 Correlation coefficient values between two normal positions (#4 and #6 in partial optical spectroscopic map) along with their slopes in the wavelength range from 630 nm to 880 nm.

	N/N		
	slope of curve 4	correlation between pts(4,6)	slope of curve 6
	-0.0027	0.99	-0.0029
	-0.0025	0.98	-0.0029
	-0.0023	0.94	-0.0022
	-0.0021	0.93	-0.0022
	-0.0024	0.99	-0.0030
	-0.0024	0.96	-0.0027
Mean	-0.0024	0.96	-0.0026

Table 3.2 shows the correlation coefficients between two spectra taken from two normal tissue positions (#4 and #6), as labeled N/N. The middle column carries the correlation values of the two normal curves i.e. curve #4 and curve #6. The mean of the R values is 0.96, strongly indicating a good correlation between the two normal curves.

The left and right columns represent the slopes of curves #4 and curve #6, respectively, with very consistent means between the two cases (or columns). Notice that the slopes here were not multiplied by 1000.

Table 3.3 Correlation coefficient values between a normal position and a tumor position (#4 and #7, #4 and #8, #6 and #7, #6 and #8 in partial optical spectroscopic map) along with their slopes in the wavelength range from 630 nm to 880 nm.

	NC											
	slope of curve 4	correlation between pts(4,7)	slope of curve 7	slope of curve 4	correlation between pts(4,8)	slope of curve 8	slope of curve 6	correlation between pts(6,7)	slope of curve 7	slope of curve 6	correlation between pts(6,8)	slope of curve 8
	-0.0027	0.33	-0.0023	-0.0027	0.01	-0.0025	-0.0029	0.15	-0.0023	-0.0029	0.54	-0.0025
	-0.0025	-0.06	-0.0021	-0.0025	0.14	-0.0022	-0.0029	0.09	-0.0021	-0.0029	0.28	-0.0022
	-0.0023	0.11	-0.0018	-0.0023	0.18	-0.0020	-0.0022	0.13	-0.0018	-0.0022	0.37	-0.0020
	-0.0021	0.32	-0.0012	-0.0021	0.38	-0.0019	-0.0022	0.46	-0.0012	-0.0022	0.18	-0.0019
	-0.0024	0.07	-0.0020	-0.0024	0.50	-0.0020	-0.0030	0.44	-0.0020	-0.0030	0.29	-0.0020
	-0.0024	-0.67	-0.0019	-0.0024	-0.79	-0.0021	-0.0027	0.14	-0.0019	-0.0027	-0.09	-0.0021
Mean	-0.0024	0.02	-0.0019	-0.0024	0.07	-0.0021	-0.0026	0.23	-0.0019	-0.0026	0.26	-0.0021

Table 3.3 represents the calculated correlations between the normal tissue curves and tumor curves along with the slopes (630-880 nm) of individual curves. The detailed information for the columns listed in this table is given below:

1. The correlation between curve #4 (normal) and curve #7 (tumor),
2. The correlation between curve #4 (normal) and curve #8 (tumor),
3. The correlation between curve #6 (normal) and curve #7 (tumor),
4. The correlation between curve #6 (normal) and curve #8 (tumor),

The means of slopes and correlation coefficients are listed in the last row. Since the normal tissue and tumor should not be related, the mean correlation value for all of them is much below 1, as expected.

Table 3.4 Correlation coefficient values between the thinnest parenchyma and a tumor position (#5 and #7, #5 and #8 in partial optical spectroscopic map) along with their slopes in the wavelength range from 630 nm to 880 nm.

	T/C					
	slope of curve 5	correlation between pts(5,7)	slope of curve 7	slope of curve 5	correlation between pts(5,8)	slope of curve 8
	2.55	0.004	2.26	2.55	0.01	2.49
	2.85	-0.23	2.09	2.85	-0.03	2.22
	1.50	0.75	1.85	1.50	0.86	2.04
	2.45	0.37	1.25	2.45	0.34	1.88
	3.39	0.14	2.03	3.39	0.29	1.97
	2.75	0.26	1.92	2.75	0.19	2.15
Mean	2.80	0.22	1.90	2.80	0.16	2.12
Stdev	0.56	0.04	0.38	0.56	0.03	0.42
SEM	0.25	0.02	0.17	0.25	0.01	0.19

Table 3.4 displays the extent of linear relation between the thinnest parenchyma and tumor, as labeled T/C, where "T" means thinnest parenchyma. For all the partial nephrectomy cases, curve #5 corresponds to the spectrum taken from the thinnest parenchyma, curves #7 and #8 are the spectra from the tumor. The highlighted row in the table represents the case having a positive margin. The mean listed in the table was calculated by excluding the positive margin case. Furthermore, Figure 3.14 presents another graphical representation for correlation between curve #5 and curve #7, showing a correlation of 0.004 (bad correlation).

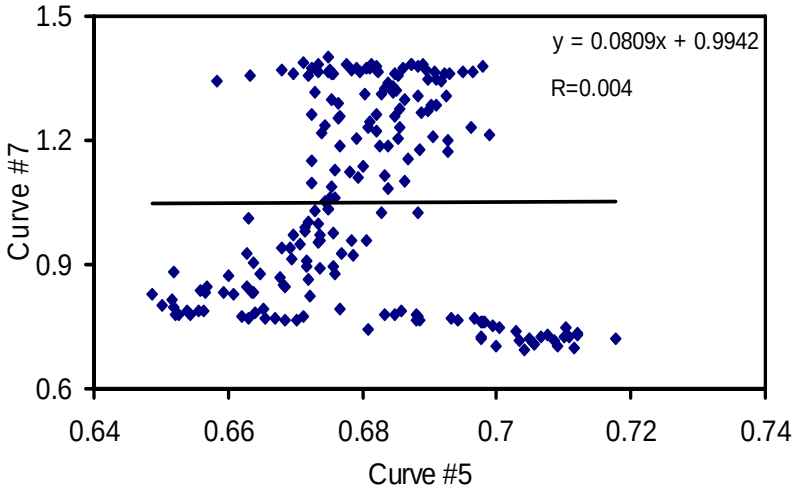

Figure 3.14 A graphical representation of the correlation calculation method between curve #5 and curve #7

Table 3.5 Correlation coefficient values between the thinnest parenchyma and a normal position (#4 and #5, #5 and #6 in partial optical spectroscopic map) along with their slopes in the wavelength range from 630 nm to 880 nm.

	T/N				
	slope of curve 4	correlation between pts(4,5)	slope of curve 5	correlation between pts(5,6)	slope of curve 6
	-0.0027	0.93	-0.0026	0.90	-0.0029
	-0.0025	0.97	-0.0029	0.93	-0.0029
	-0.0023	0.38	-0.0015	0.58	-0.0022
	-0.0021	1.00	-0.0024	0.93	-0.0022
	-0.0024	0.99	-0.0034	0.99	-0.0030
	-0.0024	0.92	-0.0028	0.93	-0.0027
Mean	-0.0024	0.96	-0.0028	0.94	-0.0026

Table 3.5 displays the correlations between the normal and thinnest parenchyma, as labeled T/N, where "T" means thinnest parenchyma. It is known that curves #4 and #6 are from the normal tissues, and curve #5 is taken from the thinnest parenchyma. The highlighted row is the case of positive margin. As seen in case of positive margin, there is a poor correlation between the normal tissue and thinnest

parenchyma because for that case, the thinnest parenchyma is well correlated with the tumor curve.

3.5.3 Results obtained for differentiation between benign tumors and malignant tumors

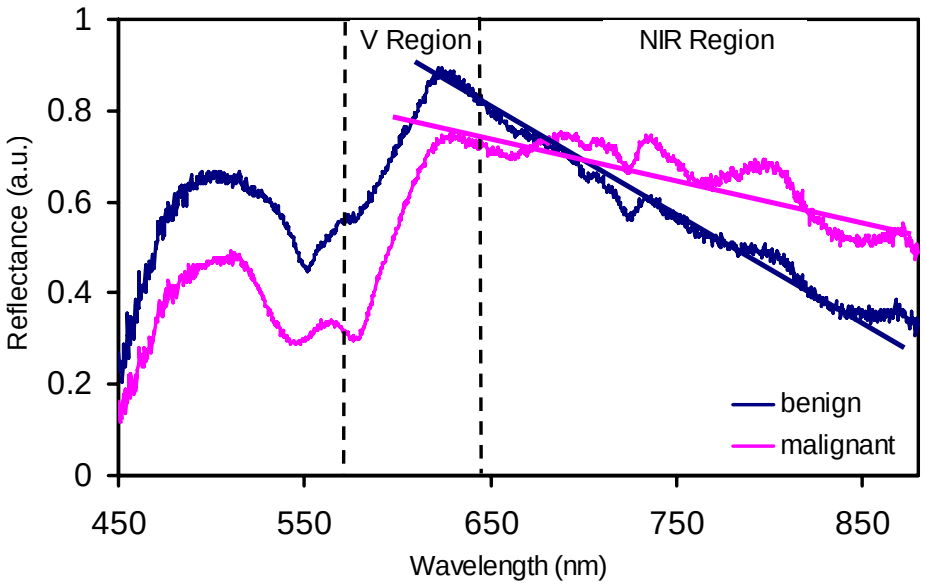

Figure 3.15 The average spectra taken from the benign tumors (blue curve, mean of 12 benign tumor sites) and from malignant tumors (pink curve, mean of 28 malignant tumor sites).

From the entire data set (n=12 for benign and n=28 for malignant tumors), six patients had tumors which were benign in nature, and the rest fourteen cases had malignant tumors. The mean of the reflectance curves of benign and malignant tumors are plotted in Figure 3.15. These curves were similarly divided into the NIR region and visible region. The slopes in the NIR region were calculated and plotted in Figure 3.16, while those in the visible region are shown in Figure 3.17. The p-value for the NIR region was found to be 0.005 after the student t-test, and that for visible region was

found to be 0.02. Since the p-value is much less than 0.05, significant differences exist in the spectral slopes of both NIR region (630-880 nm) and visible region (560-630 nm) between the benign tumors and malignant tumors.

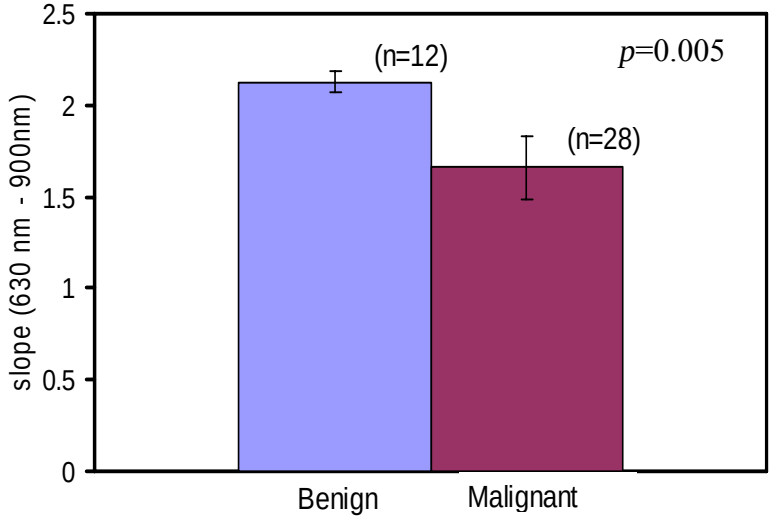

Figure 3.16 Difference in slopes in the wavelength range from 630 nm to 880 nm, obtained with the NIRS measurement from kidney samples for benign tumors and malignant tumors.

In the visible region, the correlation calculations were calculated for the benign (n=12) and malignant (n=28) tumors. The mean spectra of the reflectance from the benign (blue curve in Figure 3.15) and malignant (pink curve in Figure 3.15) tissues were used to calculate the correlation values. Table 3.6 below displays the correlation values between partial benign (PB) and radical benign (RB), partial malignant (PM) and radical malignant (RM). Finally, the correlation value is obtained between benign (B) and malignant (M), in which the partial and radical benign tumors were grouped and were named as "benign" and the same was done for "malignant". This table demonstrates the feasibility that the correlation method is an effective way to be used to differentiate benign and malignant kidney tumors, provided a known benign or

malignant sample spectrum is available. Further studies will be needed to advance this cancer identification method.

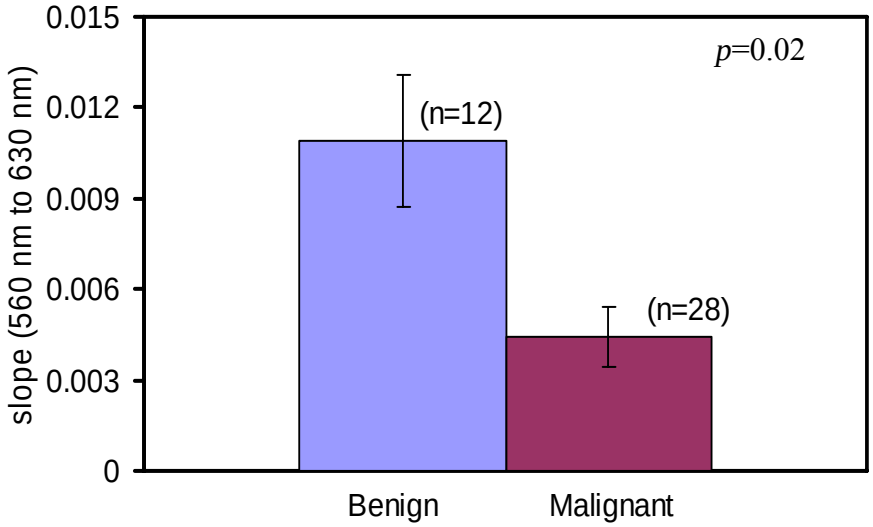

Figure 3.17 Difference in slopes in the wavelength range from 560 nm to 630 nm, obtained with the NIRS measurement from a kidney sample for benign tumors and malignant tumors

Table 3.6 Correlation coefficient values between partial benign and radical benign tumors, partial malignant and radical malignant tumors and then combined benign (partial and radical) versus combined malignant (partial and radical)

PB/RB	PM/RM	B/M
0.99	0.97	0.49

CHAPTER 4

SPECTROSCOPIC MEASUREMENTS ON THE PROSTATE SAMPLE EX-VIVO

A prostate gland is a part of the male reproductive system. In prostate cancer, the cells of prostate multiply out of control, and they metastasize to other parts of the body. Prostate cancer doesn't generally have symptoms, and hence the patient's undergo no therapy and ultimately die of other causes. Prostate cancer is often detected by Digital Rectal Examination (DRE) or by screening blood tests, such as the PSA (prostate specific antigen) test. There is some current concern about the accuracy of the PSA test and its usefulness. PSA levels under 4 ng/mL (nanograms per milliliter) are generally considered normal, while levels over 4 ng/mL are considered abnormal. However, PSA is not a perfect test. Some men with prostate cancer do not have an elevated PSA, and most men with an elevated PSA do not have prostate cancer. PSA levels can change for many reasons other than cancer. Two common causes of high PSA levels are enlargement of the prostate (benign prostatic hypertrophy (BPH)) and infection in the prostate (prostatitis)[13].

The use of DRE also has never been shown to prevent prostate cancer deaths when used as the only screening test [14].

The only test which fully confirms the diagnosis of prostate cancer is a biopsy. During this process, a biopsy gun inserts via the rectum and removes small pieces of tissue by special hollow-core needles (usually three to six on each side of the prostate) in less than a second. The tissue samples are then examined under a microscope to determine whether cancer cells are present and to evaluate the microscopic features (or Gleason score) of any cancer found. Fifty-five percent of men report discomfort during prostate biopsy [15].

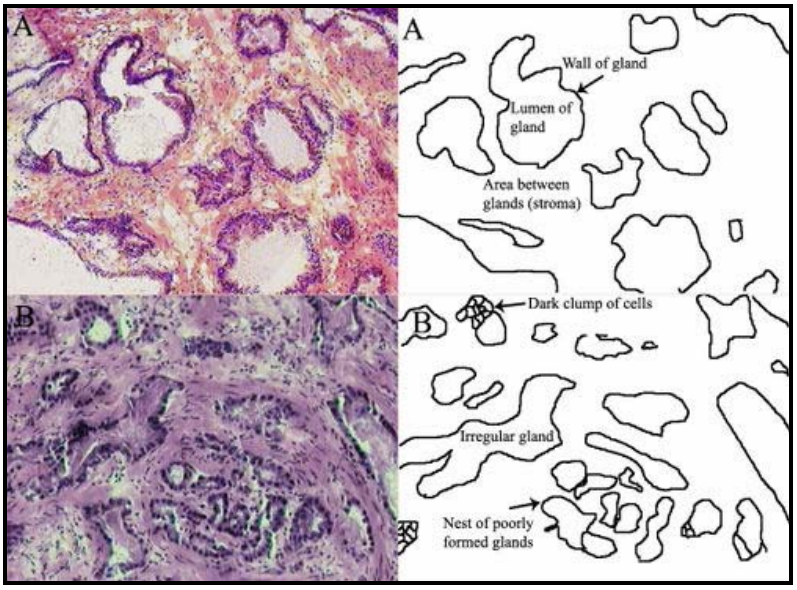

Figure 4.1 (A) Normal prostate (B) Prostate cancer. In prostate cancer, the regular glands of the normal prostate are replaced by irregular glands and clumps of cells, as seen in these pictures taken through a microscope.

Currently, an active area of research for any urologist involves non-invasive methods of prostate tumor detection and also a minimally invasive guidance tool during laparoscopic prostatectomy. Hence, my second area of application for my research project was to check whether optical (visible and NIR) spectroscopy have the potential to detect tumors in prostate gland.

The optical spectroscopic system used for prostate measurements was the same as that used for kidney sample measurements. The measurements were taken at the University of Texas Southwestern Medical Centre at Dallas, and the data processing and analysis was done at the University of Texas at Arlington. The study was approved by the Institutional Review Board of The University of Texas at Arlington and University of Texas Southwestern Medical Centre at Dallas (UTSW).

For prostate measurements, a different optical spectroscopic measurement map was used. In the preliminary testing phase, I took the initial spectroscopic measurements from several prostate samples.

After completing the laparoscopic prostatectomy, the entire prostate gland was removed along with some surrounding tissues and was put on a bucket of ice. This bucket holding the prostate sample was sent to the pathology department for further research. At the pathology department, the weight of the gland was checked, and several other measurements were done like the length of the gland from apex to base, anterior to posterior and so on. Figure 4.2 shows a photo for an ex-vivo human prostate gland with labels of posterior region, lateral region, and apex. On completion of these procedures, the prostate sample was marked with two different colors. This was done to differentiate between the right and the left side of the prostate which was basically for histology purposes (Figure 4.3).

The next step after completion of these histology formalities and procedures was optical spectroscopic measurements. To start with that, the prostate sample was bi-halved (Figure 4.3) so that the outside fibrous prostatic tissue and capsules were

bypassed, and there could be direct contact with the inside tissue through the optical probe.

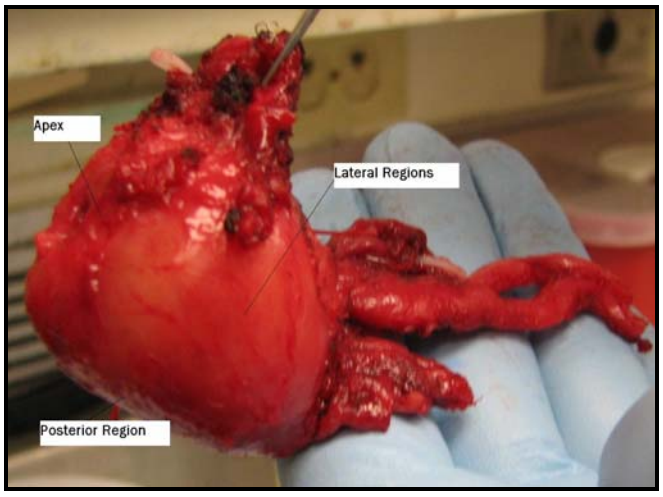

Figure 4.2 An ex-vivo prostate gland. The gland sits in the human body in the same position as shown above.

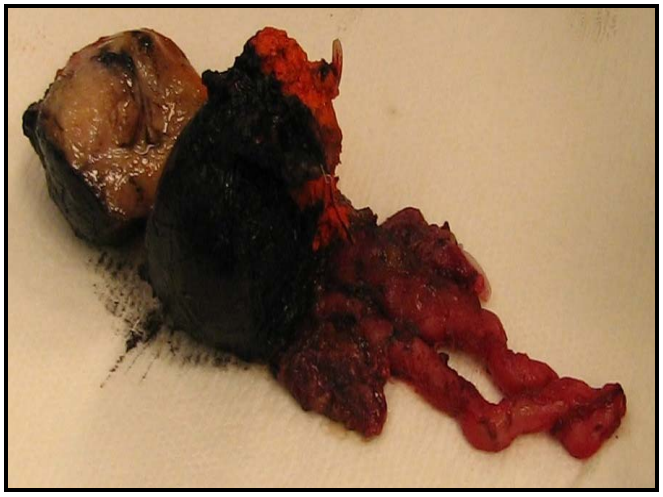

Figure 4.3 A prostate sample marked by different colors and bi-halved.

After the prostate sample was bi-halved, it was noticed that the prostate tumors were very much different as compared to kidney tumors. The kidney tumors, when being cut, looked necrotic and could be differentiated by the naked eye. But the prostate

gland was absolutely homogenous. There were no abnormalities which could be seen by the naked eye. At times, there were certain yellow spots noticed (Figure 4.4) which were a bit swollen.

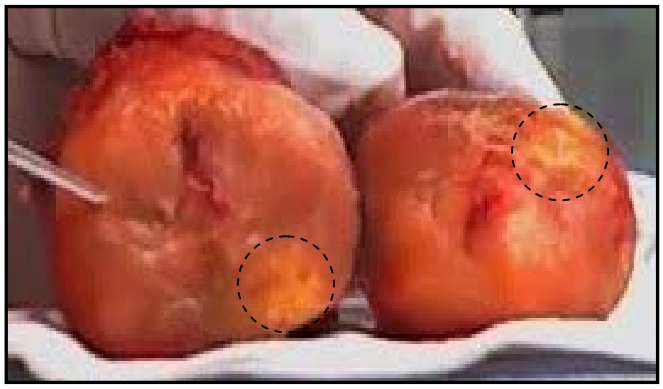

Figure 4.4 A bi-halved prostate sample displaying the swollen yellow spots.

After dividing the prostate gland into two halves, optical spectroscopic measurements were made on both sections. Unlike kidney, there was no specific map followed for my measurements. Instead, I used the labeling method given as follows:

Every section of the bi-halved was divided into four quadrants: left anterior, left posterior, right anterior and right posterior. There were no measurements made on the transition zone since it contributes the least to the whole prostate (5-10%). Most of the measurements were made on the peripheral zone. Usually, the transition zone is the origin of BPH, whereas prostate cancer can arise in any anatomical zone, although more specifically 75–85% of all prostate cancers are in the peripheral zone [16]. Hence for our optical measurements, we concentrated more on the left and right posterior sections since they represented the peripheral zone.

4.1 Data Analysis using slope measurement technique

For prostate data analysis, each case was treated independently. I did not calculate the mean across all (n=13) cases. Since prostate tumors were believed to be homogenous, it was difficult to analyze the data without the histology maps. We had histology results for two cases.

The experimental set up was same as mentioned in Chapter 2. All effects from the optical fiber, light source and spectrometer were removed by dividing each reflectance reading by a calibration curve taken from a standard reflectance surface [17]. The sample provides 100% reflectance in the wavelength range of 250 nm to 2000nm (Diffuse Reflectance Standard Specifications, Ocean Optics, FL). Before I started taking the measurements on the sample, a background measurement was recorded with the same experimental set up but with the light source switched off. By recording this background signal prior to the actual measurement and subtracting it from the raw data, we could remove the thermal effects (dark current) from the electric components and ambient light.

After subtracting the background reflectance reading and dividing by the standard white sample reflectance curve, the spectral slopes were calculated for the wavelength range from 630 nm to 900 nm. Then the mean of slopes for normal and tumor were calculated and a student t-test performed. A student t-test is a fundamental statistical process to compare the two means of two groups of data. Normally, if p is less than 0.05 ($p<0.05$), the two means of the two groups are significantly different; if $p>0.05$, the two means have no differences.

4.2 Results

4.2.1 Results obtained from Subject 1

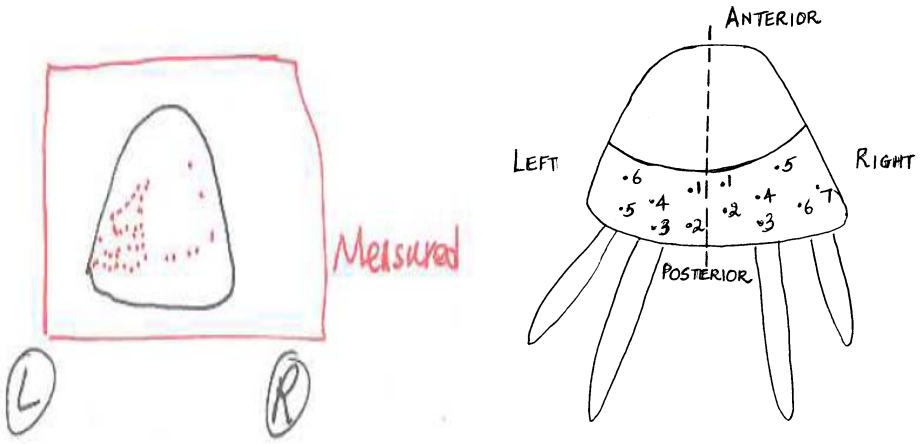

(a) (b)

Figure 4.5 (a) Histology map (b) Optical spectroscopic measurement map

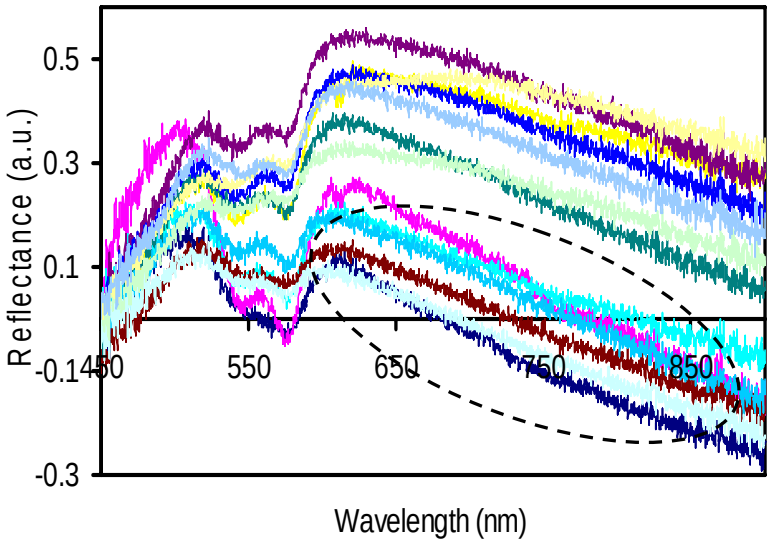

Figure 4.6 Optical reflectance curves from a prostate sample after subtracting background and dividing by white sample

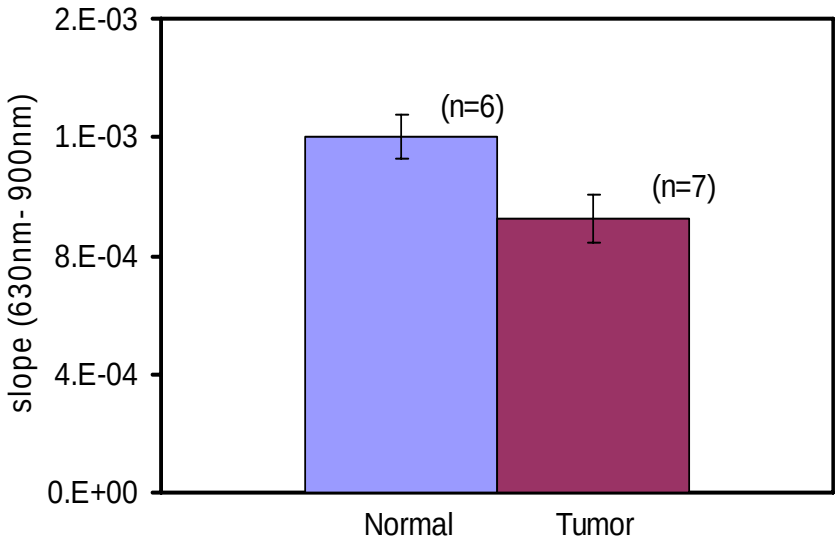

Figure 4.7 Difference in slopes in the wavelength range from 630nm to 900nm, obtained with the NIRS measurement from a prostate sample

Figure 4.5(a) displays the results obtained after histology. As shown, the left posterior region shows tumor (marked by dots). In Figure 4.5(b), a location map for this specific specimen is given with labels for the optical measurement. The optical curves highlighted with a circle in Figure 4.6 are the data taken from the left posterior region (cancer tissue), and the spectra not been included in the circle are taken from the right posterior region (for normal tissue). In our optical spectroscopic map (Figure 4.5 (b)), 6 points in the left region have been assumed as cancer according to the histology map, and the other 7 points in the right region considered as normal. The means of the NIR slopes measured from the 6 cancer points were calculated and named as "tumor". Similarly the mean NIR slopes of the 7 normal spectra yielded a curve "normal". After taking the student t-test (Figure 4.7), the p-value was found to be 0.03 which is less than

0.05. Hence there was a significant difference in NIR slope observed between "normal" and "tumor".

4.2.2 Results obtained from Subject 2

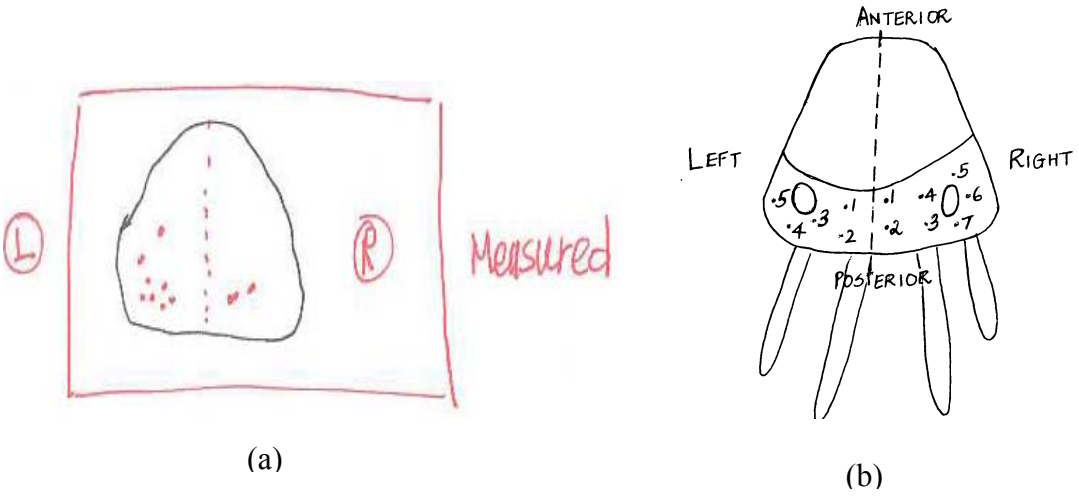

(a) (b)

Figure 4.8 (a) Histology map (b) Optical spectroscopic measurement map

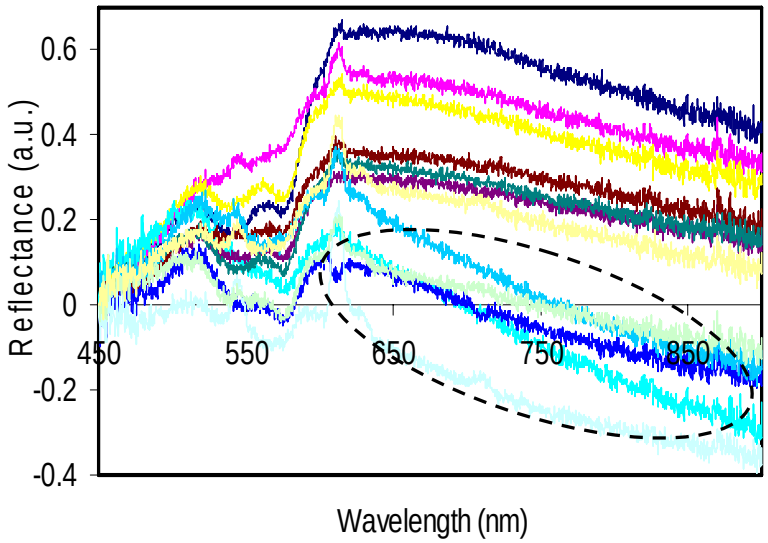

Figure 4.9 Optical reflectance curves from a prostate sample after subtracting background and dividing by white sample

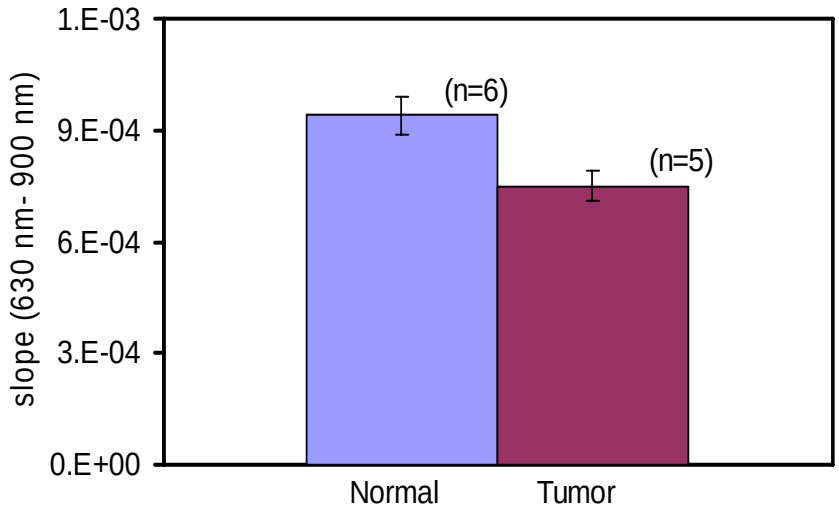

Figure 4.10 Difference in slopes in the wavelength range from 630 nm to 900 nm, obtained with the NIRS measurement from a prostate sample

The histology maps in Figure 4.8(a) is for the 2nd human specimen and shows that there is tumor in the left posterior region of the bi-halved prostate sample. The optical curves (Figure 4.9) grouped in a circle are from the left posterior region i.e. from points 1, 2, 3, 4, 5 of the left region in Figure 4.8(b), and the other curves are from points 1, 2, 3, 4, 5, 6, 7 of the right region in Figure 4.8(b). The bar graph (Figure 4.10) represents the mean of slopes from normal spots and from tumor spots. The p value calculated with the student t-test was 0.019 which states that NIRS slopes can differentiate between a normal and tumor region.

4.2.3 Results obtained from Subject 3

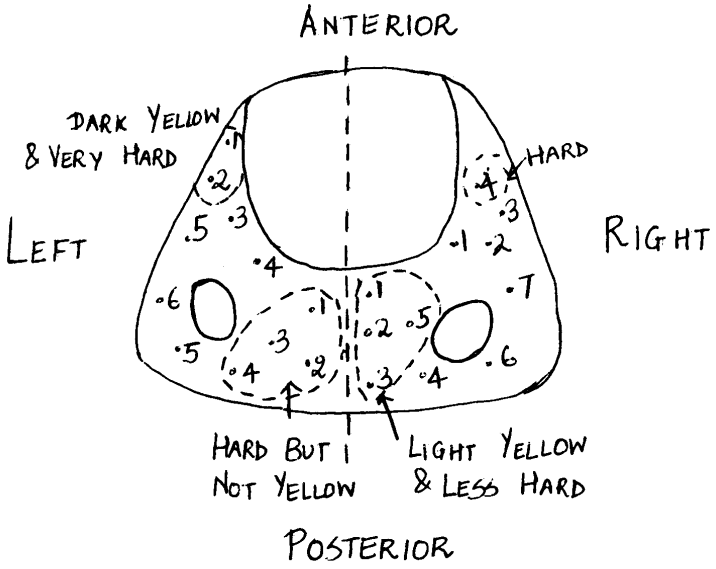

Figure 4.11 Optical spectroscopic measurement map

While taking measurements, notes were made about each point on the sample. As seen in Figure 4.11, points 1, 2 have been marked since they were dark yellow in color and were very hard to touch. Along with these notes, a pathologist used to instruct me about the possibility of a tumor at a particular place while cutting the sample. I did not have a histology map for this subject for our reference.

The optical curves shown in Figure 4.12 are obtained after calculating the mean of reflectance values for the assumed normal and tumor. For this subject, according to the notes made on the optical measurement map, the tumor is assumed to be at points 1, 2 from left anterior region, at points 1, 2, 3, 4 from left posterior region and at points 1, 2, 3, 5 from right posterior region. After taking the mean of the reflectance of these 10

points, we obtain an optical curve named as "Mean of tumor" in Figure 4.12. The "Mean of normal" is obtained by taking the mean of the rest 12 points.

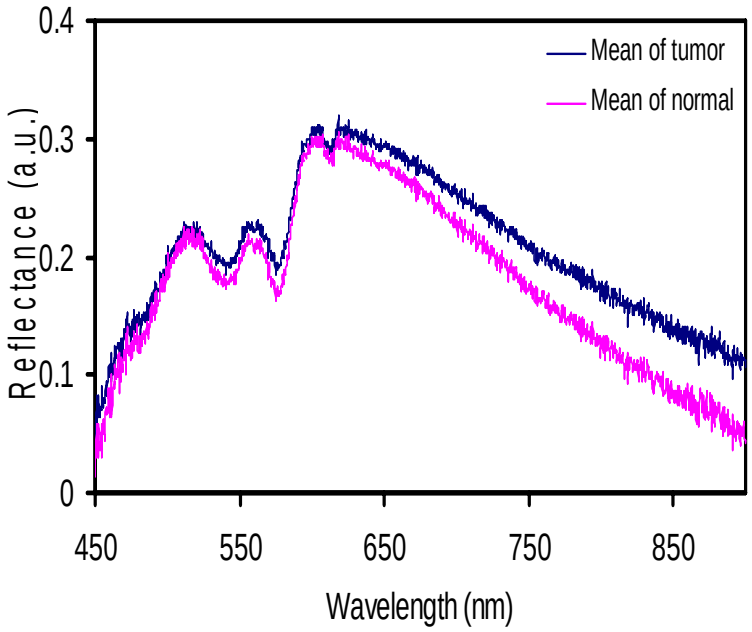

Figure 4.12 Optical reflectance curves from a prostate sample after subtracting from background and dividing by white sample

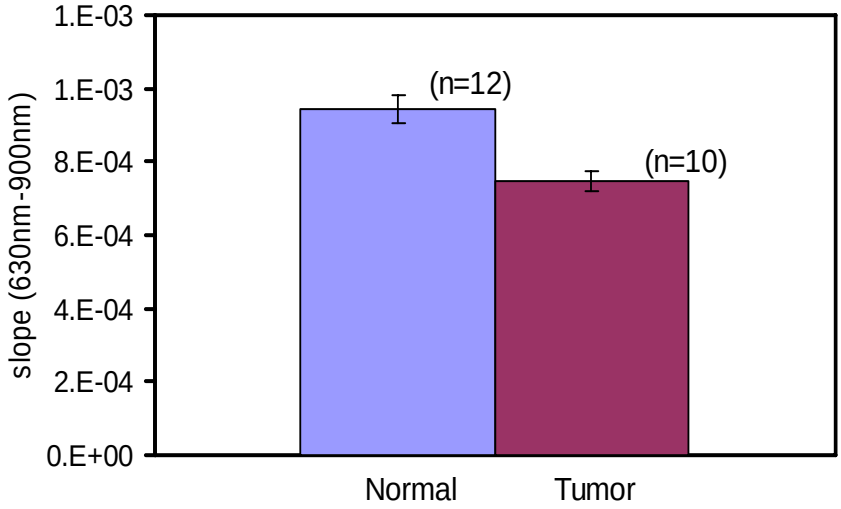

Figure 4.13 Difference in slopes in the wavelength range from 630 nm to 900 nm, obtained with the NIRS measurement from a prostate sample

Figure 4.13 is a bar graph representation of the slope calculations of "Mean of normal" and "Mean of tumor" in the wavelength range from 630 nm to 900 nm. The p-value calculated through the student t-test was found to be 0.0007, showing that there is a significant difference in NIR slopes between the normal and the tumor curve in the scattering region.

4.2.4 Results obtained from Subject 4

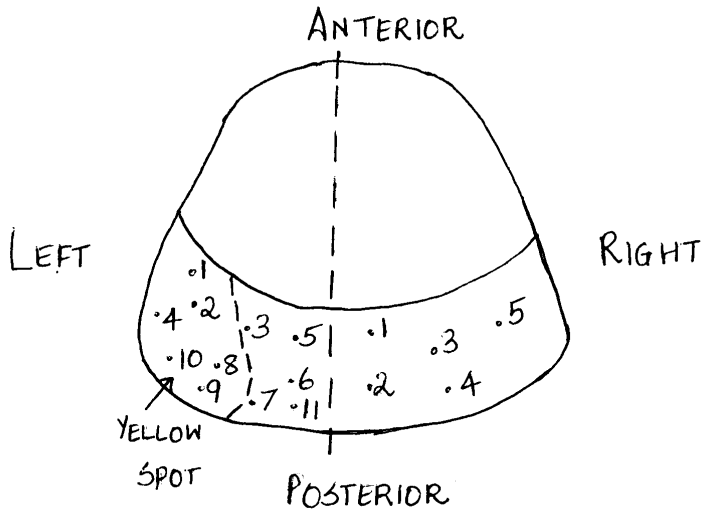

Figure 4.14 Optical spectroscopic measurement map for Subject 4

I did not have histology maps for reference for subject 4.

As shown in the optical spectroscopic map (Figure 4.14), points 1, 2, 8, 9, 10 which are highlighted are assumed to be tumors, according to the notes made during measurement. The bar graph (Figure 4.16) represents the mean of the slopes of the reflectance curves of these 5 points (Figure 4.15 grouped with a circle) for "tumor" and the mean of the slopes of the rest 10 points for "normal.

The p-value found through the student t-test was 0.012.

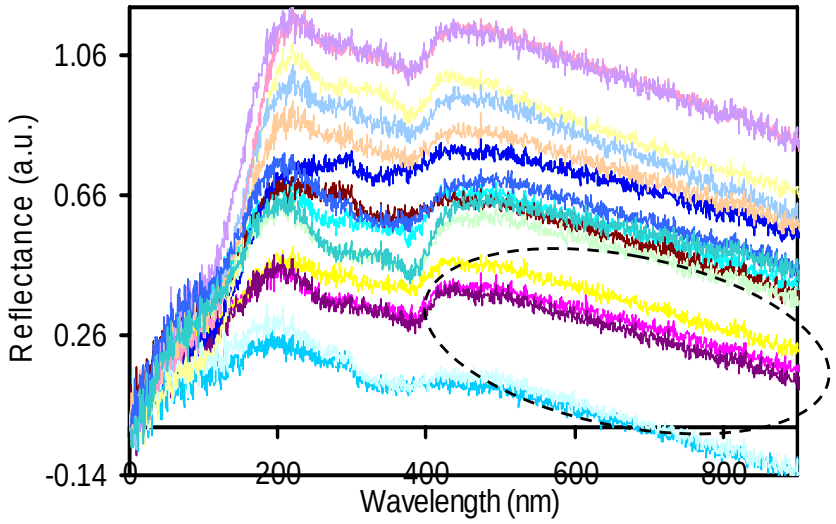

Figure 4.15 Optical reflectance curves from a prostate sample of subject 4 after subtracting background and dividing by white sample

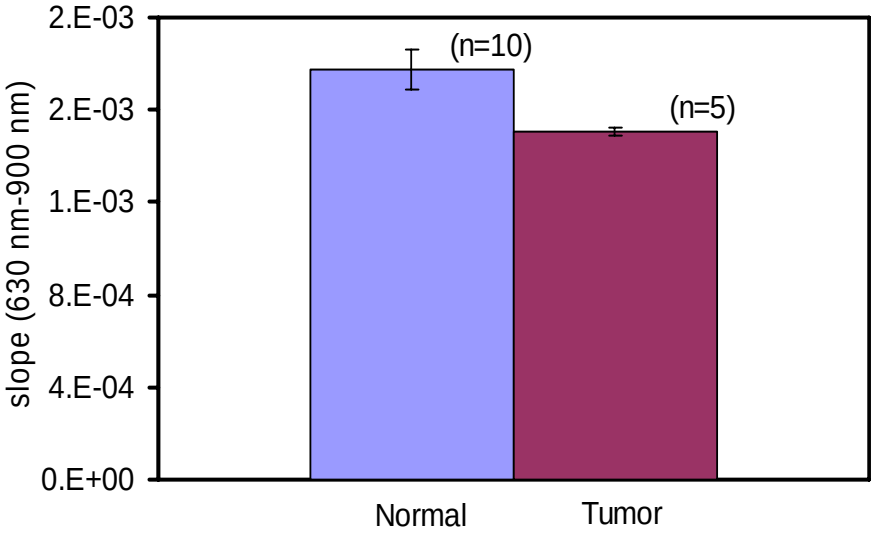

Figure 4.16 Difference in slopes in the wavelength range from 630 nm to 900 nm, obtained with the NIRS measurement from a prostate sample

4.2.5 Results obtained from Subject 5

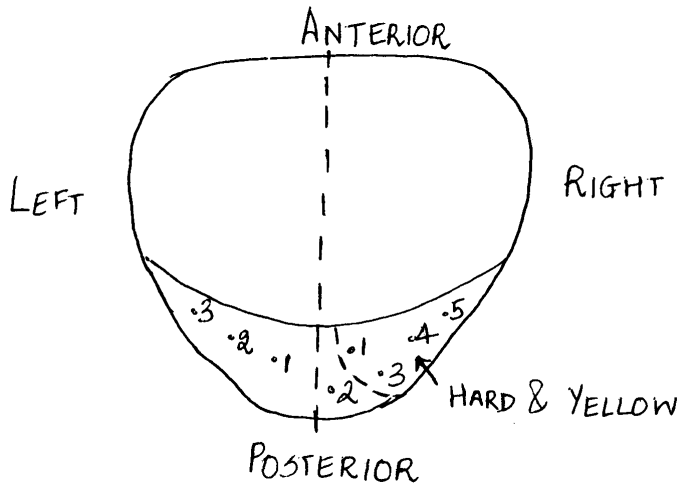

Figure 4.17 Optical spectroscopic measurement map for Subject 5

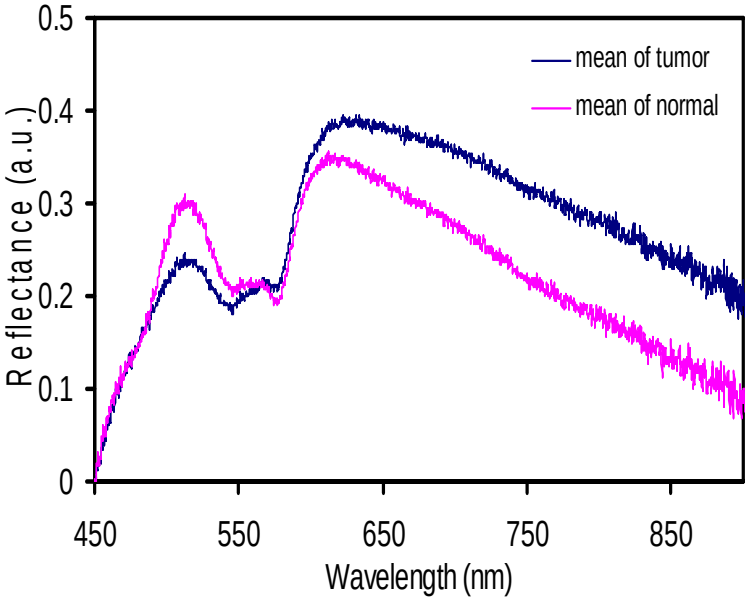

Figure 4.18 Optical reflectance curves from a prostate sample of subject 5 after subtracting background and dividing by white sample

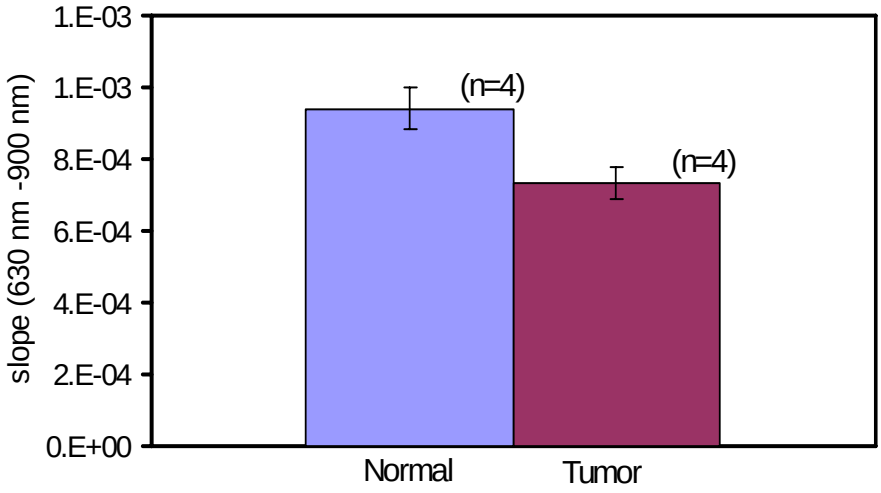

Figure 4.19 Difference in slopes in the wavelength range from 630 nm to 900 nm, obtained with the NIRS measurement from a prostate sample

I did not have histology map for subject 5 for reference.

The optical spectroscopic map (Figure 4.17) for subject 5 had points 1, 3, 4, 5 in the right posterior region which were hard and yellow in color. After calculating the slopes for these points in the wavelength range of 630 nm to 900 nm, it was found that these points had slope values less than the other points' slope values. This observation was consistent with the other 4 subjects too.

The p-value was found to be 0.033 for Figure 4.19, suggesting a statistical difference in NIR slopes between normal and tumor regions.

CHAPTER 5

DISCUSSION AND FUTURE SCOPE

Optical spectroscopy has been recognized to be a valuable tool for the detection of structural and functional changes in cells and tissues. It is based on the analysis of interactions between light and tissue. Reflectance spectroscopy has been used to explore the differentiation between normal ovary, benign neoplasms and ovarian cancer [18]. For prostate and kidney studies, various researchers have used fluorescence microscopy, Raman spectroscopy, etc to identify malignant changes. My study uses diffuse reflectance spectroscopy in which the specimens were illuminated with a broadband light source, and photons were reflected or scattered from the specimens before returning to the detector probe.

This study was to differentiate normal tissues from tumor tissues, i.e., to identify the positive margin and to differentiate benign from malignant tumors using optical spectroscopy for prostate and kidney specimens.

The results presented in this thesis show that the slope method, correlation calculation method and two wavelength classification (given in the appendix) methods have the ability to discriminate normal tissues from tumor tissues of the kidney. Slopes in the NIR and visible region provided useful discriminatory information. A p-value of 0.03 was obtained from the student t-test for kidney specimen for both NIR and visible

region (on an average for 5 specimens); a value of 0.02 was obtained for prostate specimen.

Optical spectroscopic measurements indicated that there is a difference in scattering (characterized by the NIR slopes) rather than the absorption properties between normal and cancer/tumor tissue. This is because the average size of the scattering particles is larger in tumor cells as compared to normal cells. Since most of the scattering is from the nuclei, the average size of the particle changes with the change in the size of the nuclei [19]. Tumors can contain rapidly dividing cells, non reproducing cells and necrotic cells. In all these cases, the nuclei of the cells increase in size. Hence scattering is observed more in tumor tissues.

For all the human kidney specimens, (n=48) for normal and (n=40) for tumor, there was a difference in slopes for normal tissues as compared to tumor tissues. In other words, normal tissues had a higher slope value as compared to tumor tissues in the NIR region and vice versa for the visible region. Similarly, for 5 subjects in the prostate study, the normal tissues had a higher slope value as compared to the tumor tissues. Thus we have demonstrated that in tumor, as the average size of the nuclei increases, scattering increases which is observed in the scattering region of the spectrum (630 nm to 900 nm). And as the scattering increases for tumors, there is a decrease in slope for the same in the same wavelength range.

The next challenge was to detect the positive margin for partial tumors. That was done using both the slope method and correlation coefficient method. Within an individual specimen, the correlation calculations yielded an excellent correlation for

tumor versus tumor and normal versus normal. On the other hand, there was a very poor correlation between tumoral and non tumoral tissue (r=0.07). These findings are consistent with those reported by Parekh et al who found increased reflectance measurements in 6 clear cell cancers compared to normal renal tissue between 600 and 800 nm wavelengths. Based on the empirical study and preliminary results, I have shown that reflectance spectroscopy can detect positive margin and can also differentiate benign and malignant tumors. The results showed that the partial benign and radical benign have the same slope value in the wavelength range of 630 nm to 880 nm and the same was true for partial malignant and radical malignant tumors.

For the future study, we did preliminary experiments with intralipid solution (Appendix B). Through these experiments we are trying to find several optical parameters, such as absorption (μ_a) and scattering (μ_s') coefficients, scatterer size, etc for normal tissues and tumor tissues. Also, through intralipid experiments we observed that when the intralipid concentration was kept constant and the blood quantity was increased in the intralipid solution, the slope of the reflectance curves in the wavelength range from 630 nm to 880 nm decreased. As we know, when a tumor develops, the accompanying blood supply grows with it, as does the risk of metastasis [20]. As the blood quantity increases in the intralipid solution, we expect to see more scattering which is marked by a decrease in slope.

In case of kidney, for our future study we need to compare #2 and #3 of partial kidney optical spectra (tumor through capsule in Figure3.5) with #4 and #5 of radical

kidney optical spectra (tumor through capsule in Figure 3.2). Also we can compare the readings after sectioning the tumor with those readings measured through the capsule.

This technique can be developed in an efficient manner and can have a better application for laparoscopic surgery. A probe can be designed which can enter the patients body through the holes made for laparoscopic instruments. After the surgeon finishes removing the partial part of the kidney which is a tumor, the optical probe can be made to be in contact with the tissue at different positions. Before doing this, the surgeon can take one reflectance measurement on normal kidney, and its slope would be calculated in real time which would serve as a reference reading. Then when the surgeon has the optical probe touch different positions, the slopes would be displayed real time for the individual positions. These slopes can then be compared to the reference slope reading, and accordingly it can be decided whether the individual position is a normal tissue or tumor tissue. To further check it, a real time correlation calculation can be done in the visible region, correlating the reference spectra (in 560-630 nm) and the individual spectrum from the testing tissue location. If through the slope method, a particular position is found to be having tumor, the correlation calculation method should display a poor correlation value between the reference curve and that from the particular position. In this manner, the surgeon can cut safely through the tumor without worrying about the positive margin.

Thus optical reflectance spectroscopy has the potential to provide minimally invasive diagnostic and guidance imaging tool in real time which can be less expensive

and more convenient to investigate the abnormalities. We plan to conduct further trials to increase the power of these conclusions and to verify the results.

APPENDIX A

DATA ANALYSIS USING A TWO-WAVELENGTH CLASSIFICATION METHOD

On completing slope measurement technique and correlation calculations, a two wavelength classification method was tried on the entire data set.

For the two-wavelength classification method, the data were not normalized. They were subtracted from background and divided by the white sample. Two wavelengths were randomly chosen from the entire spectrum. The reflectance intensities for these two wavelengths were plotted on the X-Y scatter plot. The first criterion for choosing the two wavelengths was selecting the two main peaks of the spectrum. The reflectance intensities of one wavelength was on X axis for both normal and tumor and those of another wavelength was on Y axis for both normal and tumor.

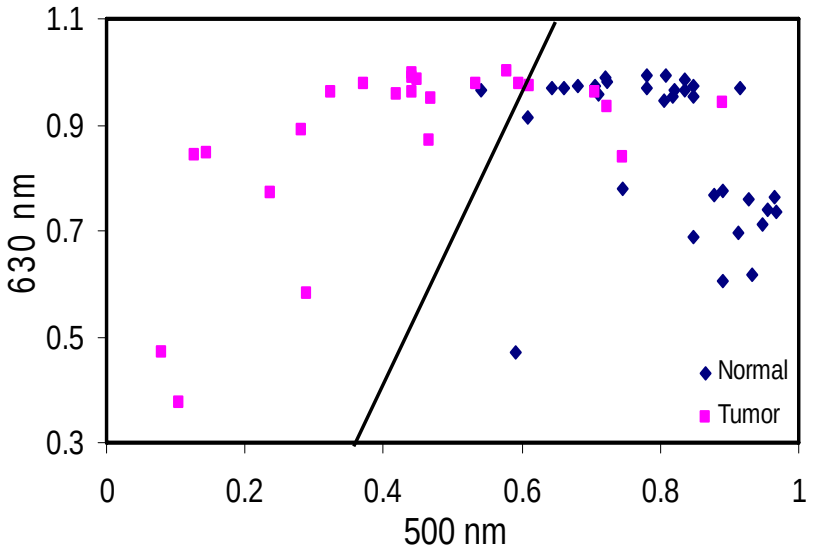

Figure 1 A two wavelength classification XY scatter plot for entire data set

In the above figure, the reflectance intensities at 500 nm for all the data points is on X axis and those at 630 nm is on Y axis. An arbitrary line was drawn which could well separate the normal tissues from tumor tissues.

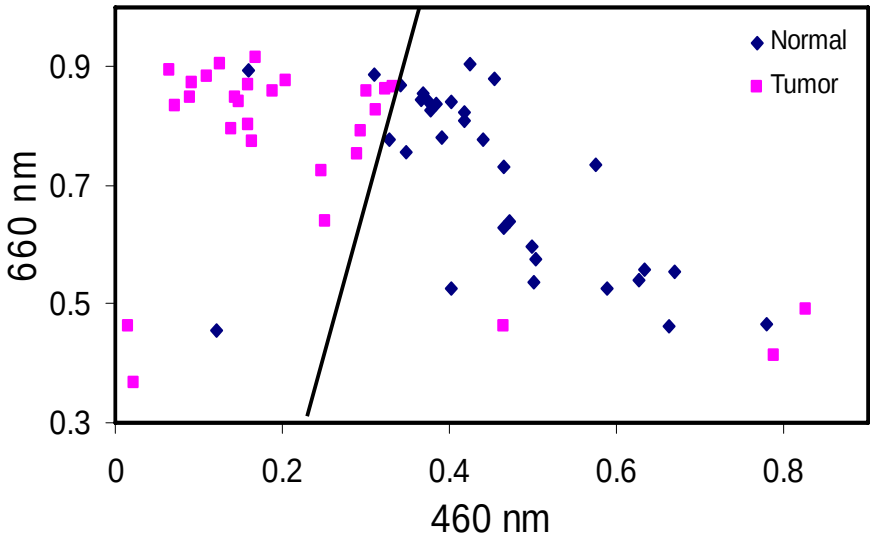

Figure 2 A two wavelength classification XY scatter plot for entire data set

X-axis represents the reflectance intensities of the entire data set at 460 nm and those at 660 nm are on the Y axis. The line drawn suggests a good classification between normal tissues and tumor tissues.

APPENDIX B

INTRALIPID DATA

The dual channel ISS oximeter (ISS, Champaign, IL) was the “gold standard” instrument used for measuring the reduced scattering coefficient from each solution. It works by emitting NIR light into the tissue at known distances from a collector. The light is measured and processed, and the absorption and reduced scattering coefficients of the medium are determined. We used two channels at 750 nm and 830 nm. Since ISS gives the absolute measurement of light absorption and scattering in highly scattering medium, it was basically used to check the accuracy of the quantity of blood added each time.

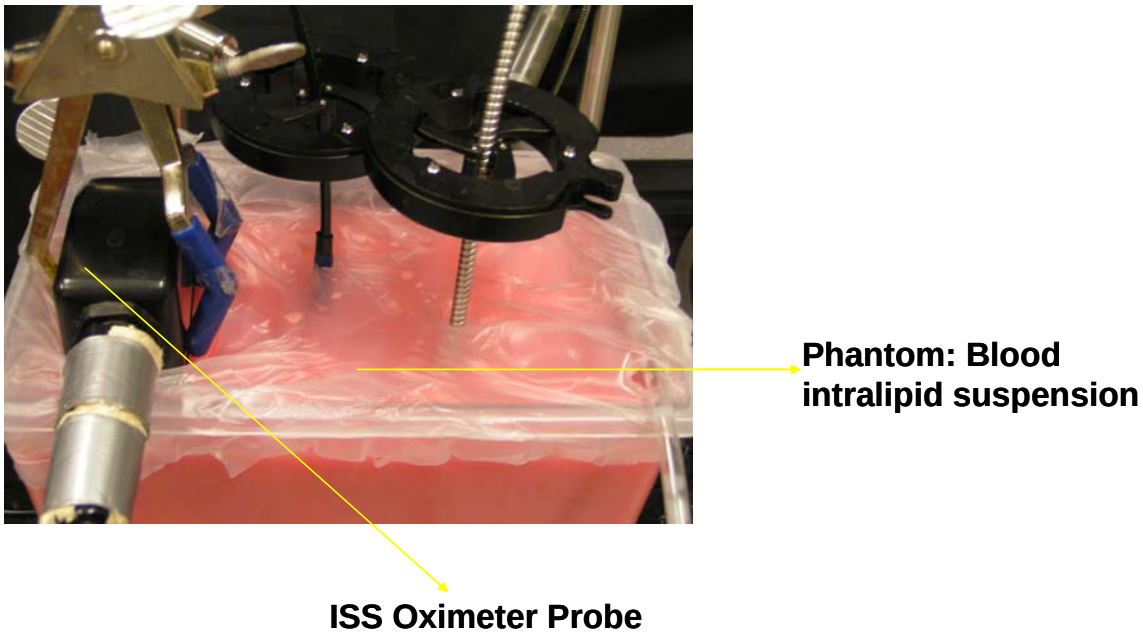

Figure 1 Experimental set up for intralipid measurements

A diluted solution of intralipid was used to simultaneously measure the reduced scattering coefficient and optical reflectance spectroscopy measurements. We choose the intralipid solution because it closely simulates light scattering properties of tissue

All measurements were done at an integration time of 50 msec. We tried it for different integration times also. The result was consistent with that of 50 msec. The intralipid solution was 20% by volume (Pharmacia and Up-John, Clayton, NC). For our measurements, we tried 3 different concentrations of intralipid ranging from 0.5% to 1.5%.

We obtained readings of μ_s' and reflectance with different concentrations of intralipid solutions using both the ISS oximeter and spectrometer, respectively. The readings were divided by the calibration curve taken from a standard reflectance sample to cancel effects from the fiber, light source and spectrometer. Both μ_s' and reflectance readings were found to be linearly proportional to intralipid concentration. The correlation coefficient (at 750 nm) was 0.98 and 0.94 respectively.

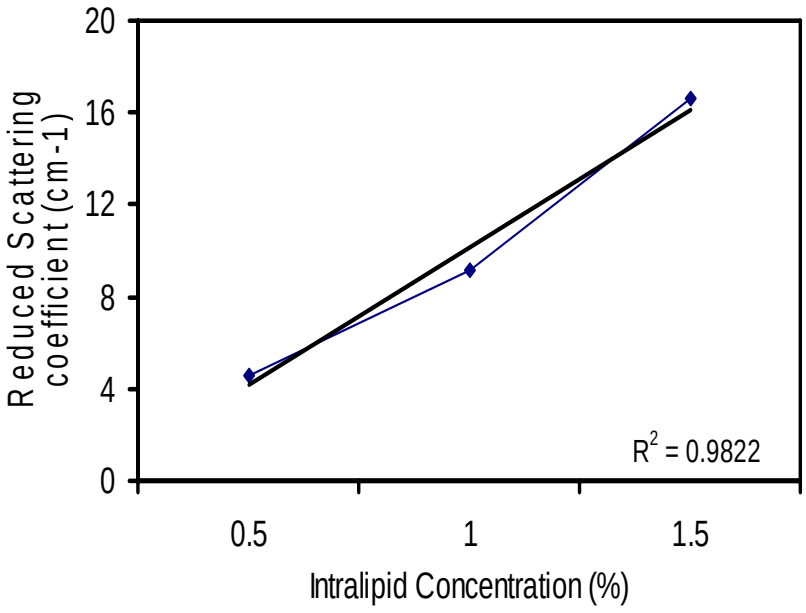

Figure 2 Linear relationship between the intralipid concentration and the μ_s' values obtained from the ISS oximeter

The slopes of the reflectance curves were then calculated in the wavelength region of 630 nm and 900 nm for different quantities of blood, but at the same intralipid concentration. It was observed that as the blood quantity increased from 10µM to 40 µM, the slope of the curve decreased.

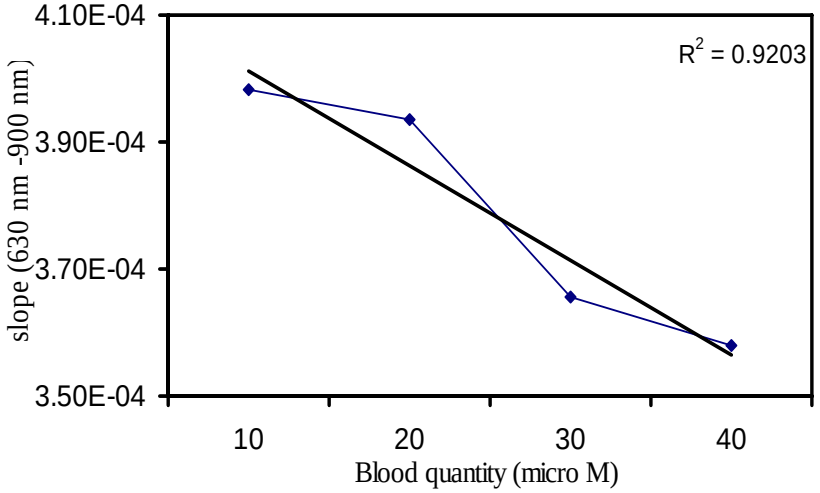

Figure 3 Relationship between the blood quantity and the slope calculated from 630 nm to 900 nm for 0.5% intralipid

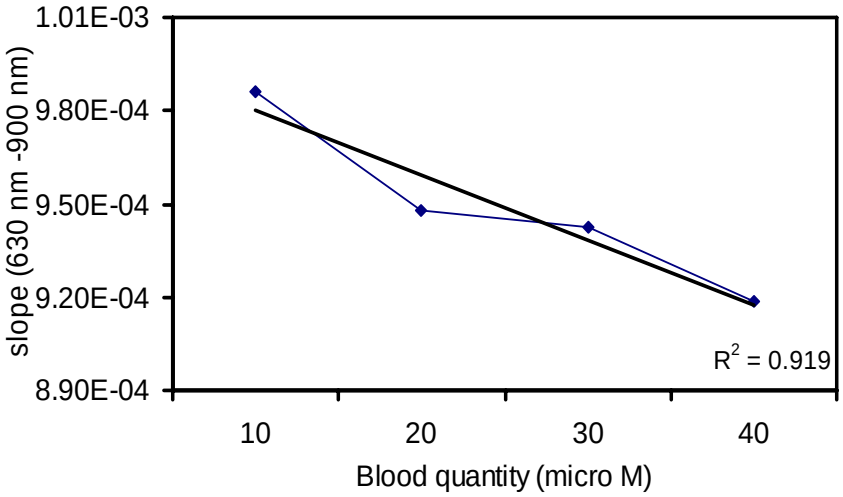

Figure 4 Relationship between the blood quantity and the slope calculated from 630 nm to 900 nm for 1% intralipid

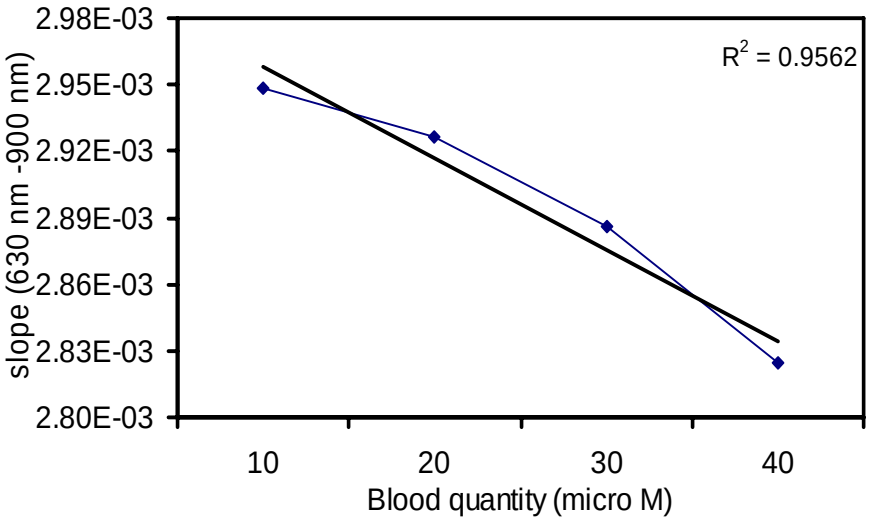

Figure 5 Relationship between the blood quantity and the slope calculated from 630 nm to 900 nm for 1.5% intralipid

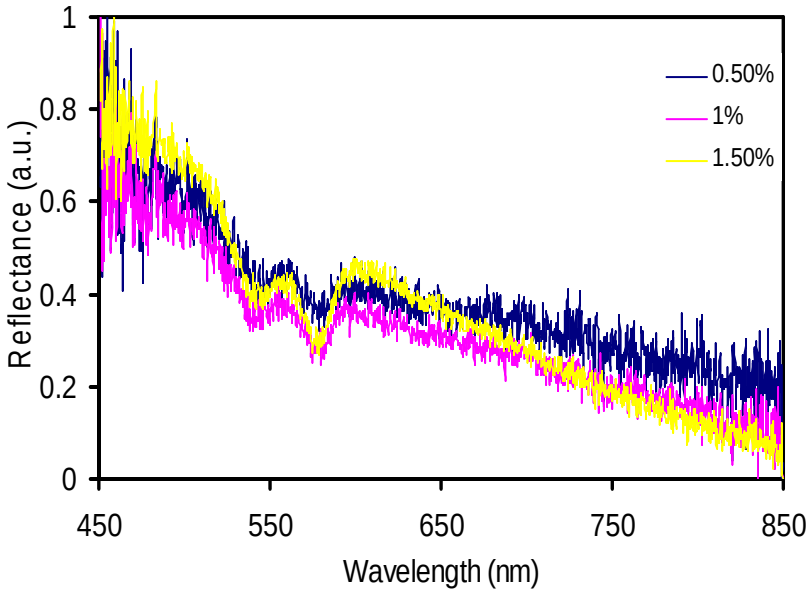

Figure 6 Normalized optical curves at 10μM blood and different intralipid concentrations

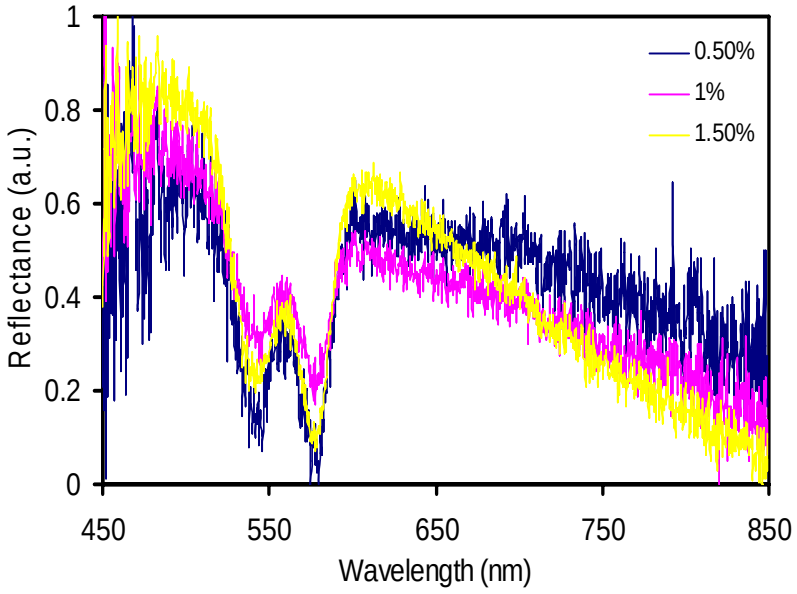

Figure 7 Normalized optical curves at 20µM blood and different intralipid concentrations

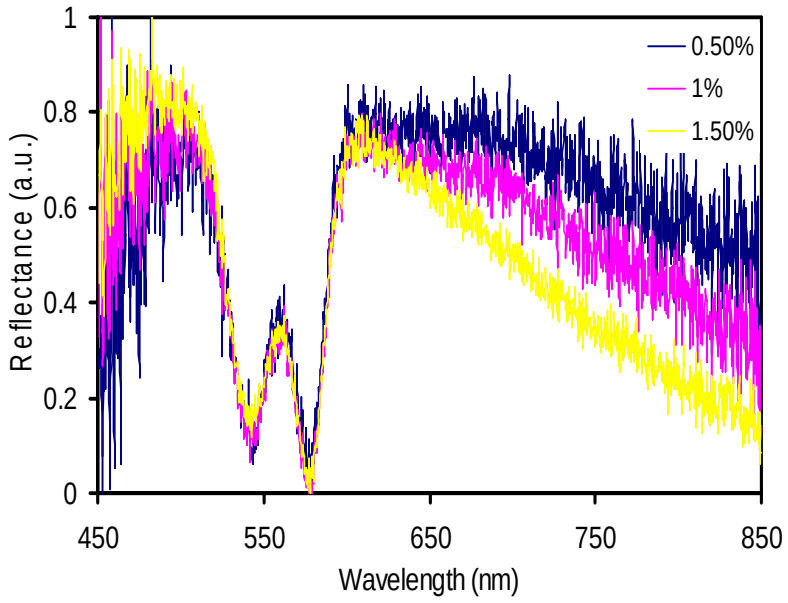

Figure 8 Normalized optical curves at 30µM blood and different intralipid concentrations

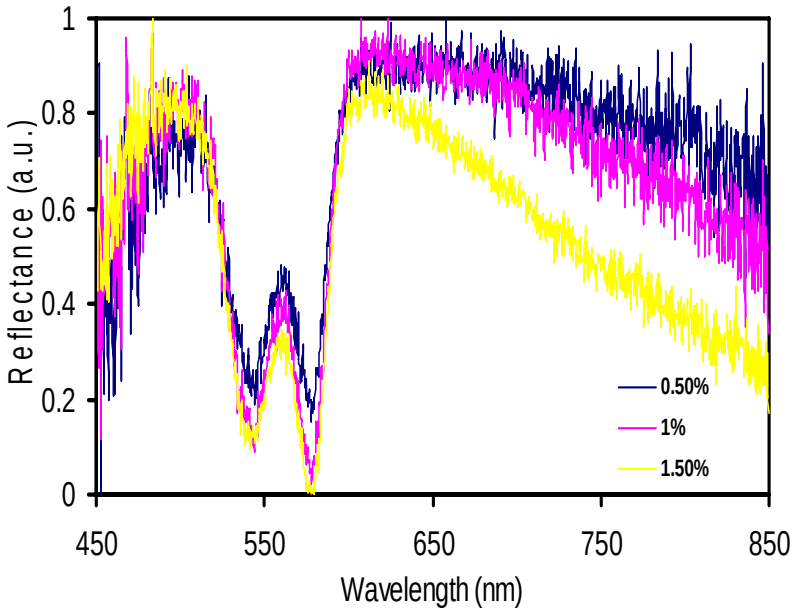

Figure 9 Normalized optical curves at 40µM blood and different intralipid concentrations

REFERENCES

[1] Website of Wikipedia : http://en.wikipedia.org/wiki/Kidney

[2] Website of Cancer Help : http://www.cancerhelp.org.uk/help/default.asp?page=4048# radical

[3] Website of Prostate Cancer : www.prostatecancercentre.co.uk/theprostate.html

[4] Website of Wikipedia : http://en.wikipedia.org/wiki/Prostate

[5] Website of General Information about Prostate Cancer : www.meb.uni-bonn.de/cancer.gov/CDR0000062965.html

[6] Website of Wikipedia : http://en.wikipedia.org/wiki/Near_infrared_spectroscopy

[7] Website of Washington State University for Near Infra Red Spectroscopy : http://postharvest.tfrec.wsu.edu/pgDisplay.php?article=J10I1B

[8] Website of Biomedical Optics Research Laboratory http://www.medphys.ucl.ac.uk/research/borl/research/NIR_topics/nirs.htm

[9] Website of Prostate Cancer : http://www.pueblo.gsa.gov/cic_text/health/prostate/prostate.html

[10] Website of Ocean Optics : http://oceanoptics.com/

[11] M. Johns, C. Giller, D. German, and H. Liu, "Determination of reduced scattering coefficient of biological tissue from a needle-like probe," Opt. Express **13**, 4828-4842 (2005)

[12] Website of Wikipedia : http://en.wikipedia.org/wiki/Correlation

[13] Website of Wikipedia : http://en.wikipedia.org/wiki/Prostate

[14] Krahn, MD; Mahoney JE, Eckman MH, Trachtenberg J, Pauker SG, Detsky AS (Sep 14 1994). "Screening for prostate cancer.. A decision analytic view". JAMA 272 (10): 773-80.

[15] Essink-Bot, ML; de Koning HJ, Nijs HG, Kirkels WJ, van der Maas PJ, Schroder FH (Jun 17 1998). "Short-term effects of population-based screening for prostate cancer on health-related quality of life". J Natl Cancer Inst 90 (12): 925-31.

[16] A. Erbersdobler, H. Augustin, T. Schlomm, and R.-P. Henke, "Prostate cancers in the transition zone: Part 1; pathological aspects," *BJU International*, vol. 94, pp. 1221-1225, 2004.

[17] M. Johns, C.A. Giller, and H. Liu, “Determination of hemoglobin saturation in blood-perfused tissues using reflectance spectroscopy with small source-detector separations,” Appl. Spectrosc. 55, 1686-1694 (2001).

[18] M. B. Urs Utzinger, Elvio Silva, David Gershenson, Robert C. Blast Jr., Michele Follen, Rebecca Richards-Kortum,, "Reflectance spectroscopy for in vivo characterization of ovarian tissue," *Lasers in Surgery and Medicine*, vol. 28, pp. 56-66, 2001.

[19] A. H. H. Judith R. Mourant, Angelia A. Eick, Tamara M. Johnson, James P. Freyer,, "Evidence of intrinsic differences in the light scattering properties of tumorigenic and nontumorigenic cells," *Cancer Cytopathology*, vol. 84, pp. 366-374, 1998.

[20] Website of Care Magazine : http://www.managedcaremag.com/archives/0401/0401.biotech.html

BIOGRAPHICAL INFORMATION

Disha Peswani was born on May 17th, 1982 in Mumbai, India. She received her Bachelor of Engineering Degree in Biomedical Engineering from Mumbai University, India in August 2004. For one year she worked as a biomedical engineer at P.D.Hinduja National Hospital and Medical Research Center and Bhatia Hospital located at Mumbai.

In fall 2005 she started her graduate studies in Biomedical Engineering from Joint Program of Biomedical Engineering at the University of Texas at Arlington and University of Texas Southwestern Medical Center at Dallas, completing it by summer 2007. Her research interests include medical imaging instrumentation and techniques and image processing.